Skolkovo Institute of Science and Technologies

as a manuscript

Vladimir P. Drachev

PLASMONIC NANOSTRUCTURES FOR OPTICAL METAMATERIALS

Dissertation Summary

for the purpose of obtaining academic degree

Doctor of Sciences in Physics

Moscow 2021

Introduction: motivation, ultimate goals, and specific tasks

A phenomenon relevant to a surface electromagnetic wave propagating at the interface between two media possessing permittivities with opposite signs, metal-dielectric interface, is a surface plasmon polariton (SPP). An external electromagnetic wave might excite the oscillation of free electrons in a metallic particle called localized surface plasmons, whose resonance frequency is the plasmon frequency dependent on the size and, mainly, the shape of the particle. The electromagnetic field is enhanced in the close vicinity to the surface of the particle or metal-dielectric boundary.

Negative-index materials (NIMs) have a negative refractive index so that the phase velocity is pointed against the flow of energy. There are no known naturally occurring NlMs in the optical range. Nevertheless, NIMs can be realized with artificially designed materials (metamaterials). Metamaterials open new avenues to achieve unprecedented functionality unattainable with naturally existing materials, as was first described by Veselago in his seminal paper ([1] Veselago, 1968). Optical NlMs (ONlMs) promise to create entirely new prospects for controlling and manipulating light, optical sensing, nanoscale imaging, and photolithography.

A possible design of such materials was repeatedly discussed in the literature mainly for the microwave spectral range ([2] Lagarkov, Sarychev, Vinogradov 1984). In particular, there were derived formulas necessary for developing materials with elongated conducting inclusions (sticks) having $\varepsilon < 0$. Later, Lagarkov et al. 1997 [3] experimentally demonstrated materials with both negative, permeability (μ) and permittivity (ε) in the microwave spectral range, and derived corresponding formulas. It seems that the first materials purposely synthesized to verify a number of effects predicted in [1] were obtained by J.B. Pendry et al. 1999 [4, and references therein].

Extensive literature presents discussion on the form of constitutive equations in electrodynamics Vinogradov et al. 1996 [5], Vinogradov 2002 [6]. In particular, to solve the dispersion equation $k^2 = k_0^2 \varepsilon(\omega, k)\mu(\omega, k)$ we must define the square root as a regular single-valued function.

To do this it suffices to take a cut along the negative real axis and calculate the square root for the permittivity and permeability of the medium separately (Lagarkov, Kisel 2001 [7]): $k = k_0\sqrt{\varepsilon(\omega, k)}\ \sqrt{\mu(\omega, k)}$. Defining the square root in this way ensures physically correct solutions for active and passive media. These works made possible to state that there are both, technologies for fabrication such materials and computational methods for predicting and designing materials having negative real parts of the permittivity ε' and permeability μ'. It has become possible to predict such materials also in the case of dissipative media.

Proof-of-principle experiments ([8] Smith et al., 2000; [9] Shelby et al., 2001) have shown that metamaterials can act as NIMs at microwave wavelengths. A large amount of attention to NIMs has been initiated by Pendry, who revisited a NIM-based Veselago superlens [1], which allows an imaging resolution which is limited only by material quality ([10] Pendry, 2000). The near-field version of the superlens has been reported then by the Zhang and Blaikie groups ([11] Fang et al., 2005; [12] Melville and Blackie, 2005).

While negative permittivity $\varepsilon' < 0$ ($\varepsilon = \varepsilon' + i\varepsilon''$) in the optical range can be attained for metals, there are no naturally occurring materials with a magnetic response at such high frequencies. Terahertz frequency experiments showed that a magnetic response and negative permeability $\mu' < 0$ ($\mu = \mu' + i\mu''$) can be accomplished ([13] Linden et al., 2004; [14] Yen et al., 2004; [15] Zhang et al., 2005). An optical metamaterial with the negative refractive index at 1.5 μm, based on paired metal nanorods embedded in a dielectric was designed in 2002 ([16-17] Podolskiy, Sarychev, Shalaev, 2002, 2003, and [18] Podolskiy et al., 2005). Then it was experimentally demonstrated in our work, which is included in this thesis ([19] Shalaev et al., 2005; [20] Drachev et al., 2006; [21] Kildishev et al., 2006).

This brief review clearly indicates a great interest to plasmonic nanostructures at the beginning of the century, explains relevance of our work, and multiple reasons for the interest growing. The main goals of the efforts presented in the thesis were experimental feasibility study on optical NIMs, metamagnetics across the visible spectral range, subdifraction photolithography using hyperbolic metamaterials, scattering suppression for microspheres with epsilon near-zero fractal shell, and effect of nano-structuring on the metal dielectric function. We have demonstrated, for the first time, feasibility of optical NIMs and losses full compensation with gain for NIMs. We should highlight also our counterintuitive experimental finding of a new type of plasmonics in magnetic nanoparticles with spin-polarization.

MAIN RESULTS

In the thesis we demonstrate in the experiments the feasibility of optical NIMs, metamagnetics across the visible spectral range, subwavelength photolithography using hyperbolic metamaterials, scattering suppression of microspheres with epsilon near-zero fractal shell, and effect of nanostructuring on the metal dielectric function. We have demonstrated, for the first time, applicability of optical NIMs due to losses full compensation with gain for NIMs. We highlight our finding of a new type of plasmonics in magnetic nanoparticles with spin-polarization.

The dissertation includes five chapters. I. Dielectric function of noble metals in plasmonic nanostructures and size effect in nonlinear response; II. New mechanism of plasmons specific for spin-polarized nanoparticles; III. Optical metamaterials with magnetism, negative refractive index, and loss compensation; IV. Sub-wavelength patterning in hyperbolic metamaterials by volume plasmon polaritons; V. Scattering suppression by epsilon-near-zero plasmonic fractal shells.

DEFENDED PROVISIONS

1. The Ag dielectric function for moderately sized, about 100 nm, strips differ from that of bulk Ag and is size-dependent for both polarizations of light. The geometrical effect of roughness is mostly responsible for increased losses at the plasmon resonances of the nanostructure, while the surface roughness does not affect the Ag permittivity. Anisotropy in ε_m'' observed in the

experiments indicates a significant contribution from the quantum size effect and the chemical interface effect.

2. Effect of annealing on the nanostructure performance depends on the geometry, and can be positive or negative. In the case of square shape nanoantennas, annealing increases the grains size and, also, reduces the reflection coefficient of the potential barriers between grains. Both factors result in substantially improved electron relaxation rate for nanostructures and make it comparable with the large area samples. Loss factor was introduced in the modeling of the gold permittivity. When the annealing temperature increases from the room temperature to $400^{\circ}C$, the loss factor decreases from 3.54 to 1.35, where factor 1 corresponds to the bulk gold.

3. (a) Analysis of the available in the literature experimental data on the nonlinear susceptibility was compared with the existing theoretical models in order to resolve the origin of the optical nonlinearity in plasmonic nanoparticles. Based on the $\chi^{(3)}$ values and its size dependence it was concluded that the conduction electron intra-band transitions play a major role, in contrast to the common belief about negligible role of the conduction electrons.

(b) Our results prove that the Rautian's model quantum well theory with the Hamiltonian of electron-field interaction taking the form *of* the dipole moment and the electrical field well suited to describe experimental the size-dependent $\chi_m^{(3)}$. The result that cannot be achieved with a theoretical size dependence derived by Hache, Ricard, and Flytzanis, with the Hamiltonian that uses a description in terms of a vector potential and electron momentum.

(c) We prove the importance of saturation effects for the local field enhancement factor, which strongly affects nonlinear processes and SERS. Therefore, the saturation will be especially important when using high-intensity laser light typical for pulsed fs and ps lasers.

4. Cobalt nanoparticles synthesized by high temperature reduction of cobalt salt show strong plasmon resonance at 280 nm with better quality than that of gold nanoparticles in the visible spectrum. Our experiments with Co nanoparticles clearly show a new type of plasmon excitation, which is specific for spin polarized single domain nanoparticles. We interpret unusual properties Co nanoparticles as a result of existence of two independent groups of electrons with opposite spins. In fact, our results show an optical analogous of giant magneto-resistance (GMR).

5. For an array of pairs of parallel gold rods, we obtained a negative refractive index of $n' \approx -0.3$ at the optical communication wavelength of 1.5 μm. It was the first experimental demonstration of optical NIMs in this competitive field.

6. Feasibility of metamagnetics in the visible spectral range was demonstrated for a grating of the nanostrips pairs. We show strong magnetic resonant behavior in all the samples ranging from 491 nm to 754 nm, covering the majority of the visible spectrum. The permeability ranges from -1.6 at 750 nm to 0.5 at 500 nm.

7. Negative refractive index has been demonstrated at the optical wavelengths using paired crossed gratings arrays (fishnets). It has been used to demonstrate a double negative-NIM response at wavelengths as short as 813 nm. The sample showed a maximum FOM (figure of merit) of 1.3 with $n' \approx -1.3$. We have also reported the shortest wavelength at which NIM behavior has been

observed. The sample displayed a single negative-NIM response at 710 nm with a maximum FOM of 0.5 with $n' \approx -0.6$.

8. (a) We have experimentally demonstrated an active negative-index metamaterial. Our results for the first time solve the inherent problem of loss in negative-index metamaterials made from nanostructured metal-dielectric composites.

(b) The strength of the loss compensation in our sample arises from the local-field enhancement of the structure when a gain medium is embedded as a spacer layer. Measured effective amplification is $\alpha = -1.07 \times 10^5 cm^{-1}$, which is 46 times larger at this wavelength than the "seed" value (without the local-field factor) that was used in simulations.

9. We have experimentally shown that diffracted light propagates inside a hyperbolic material made of a planar silver-silica lamellar structure along the resonance cone boundary between the directions with $\mathrm{Re}\,\varepsilon(\varphi_c) > 0$ and $\mathrm{Re}\,\varepsilon(\varphi_c) < 0$. Such propagation across the real metal-dielectric interfaces is a characteristic feature of the volume plasmon-polaritons (VPPs). The interference of VPPs from a double-slit creates a sub-wavelength interference pattern, which is six times smaller than the free space wavelength at 465 nm. This is in sharp contrast to the double-slit experiment in silica, which results in a diffraction-limited pattern. Such unique subwavelength interference patterns offered by hyperbolic metamaterials allow for applications in nano-photolithography demonstrated in our work.

10. (a) It is shown that the optical response of the core-shell microsphere with a gold fractal shell is dominated by the shell absorption. Similar to the planar fractal films, the absorption is enhanced in the broad spectral range up to $20\,\mu\mathrm{m}$. Nevertheless, the specular reflection and back-scattering are relatively small for the fractal shells due to 3D spherical geometry.

(b) The resulting transmission cross-section for a microsphere with gold shell is higher than the bare silica core at the Mie resonance wavelength. This is due to the forward scattering suppression of silica microspheres caused by adding the plasmonic gold shells. We prove that the absorption in the shell contributes the most to the extinction of the whole core-shell microsphere.

(c) The Mie scattering resonance at 560 nm of a silica core with 780 nm diameter is suppressed by 75% and partially substituted by the absorption in the shell so that the total transmission is increased by factor of 1.6 due to the gold fractal shell.

(d) The calculated effective permittivity of the gold shell manifests the epsilon-near-zero condition over the whole spectral range under study. The O-Si-O vibrational stretching band of the core in the mid-infrared spectral range, is "invisible" in the spectra of the core-shell extinction. These observations for the visible and mid-IR spectra indicate that the light goes mostly through the epsilon-near-zero shell with approximately wavelength independent absorption rate. Thus the fractal films being synthesized on the microspheres show interesting properties of "guiding" light through the shell.

Author contribution in the dissertation materials and defended statements is significant. Typically, it includes supervising students on their experimental work; a guidance in assembling the set-up; planning the experiments and partly the numerical simulations and fabrication; results analysis; writing manuscripts. Out of cited below papers: 10 - as a first author, 12 - as a leading author, and 8 – as a second after Ph.D. student author.

NOVELTY

We present for first time the experimental realization on optical NIMs, metamagnetics across the visible spectral range, subwavelength photolithography using hyperbolic metamaterials, scattering suppression of dielectric microsphere with epsilon near-zero fractal shell, and effect of nano-structuring on the metal dielectric function. We have demonstrated, for the first time, feasibility of optical NIMs and losses full compensation with gain for NIMs. We should highlight also our finding of a new type of plasmonics in magnetic nanoparticles with spin-polarization.

ACKNOWLEDGEMENTS

These works are combined efforts of a great team, gifted students and experienced colleagues. I greatly appreciate opportunity to work together and deeply thank all the co-authors on the cited papers for their valuable contributions.

PUBLICATIONS AND RESULTS APPROBATION

There are 77 papers to the plasmonic nanostructures, published by the author with colleagues, indexed in Scopus, WoS, and 12 invited chapters.
Among them, 35 papers are published on the thesis topics (A1-A35), as well 45 invited conference talks (B1-B45) and 29 invited lectures for Russian academic institutes and USA Universities (C1-C29).

JOURNAL PAPERS OF Q1-Q2 LEVEL (journal impact factor IF and quartile number are shown after each reference)**:**

A1. H. Bhata, A.E. Aliev, and **V.P. Drachev**, New mechanism of plasmons specific for spin-polarized nanoparticles. ***Scientific Reports*** *9, 2019 (2019). DOI:10.1038/s41598-019-38657-w. (IF4.38; Q1)*

A2. D. P. Lyvers, M. Moazzezi, V. C. de Silva, D. P. Brown, A. M. Urbas, Y. V. Rostovtsev, and **V. P. Drachev**, Cooperative bi-exponential decay of dye emission coupled via plasmons. Scientific Reports 8: *(*2018*) 9508 | DOI:10.1038/s41598-018-27901-4. (IF4.38; Q1)*

A3. K. M. Roccapriore, D. P. Lyvers, D. P. Brown, E. Poutrina, A. M. Urbas, T. A. Germer, **V. P. Drachev**, Waveguide Coupling via Magnetic Gratings with Effective Strips, **Applied Sciences,**

Section: Nanotechnology and Applied Nanosciences, Special issue "Metasurfaces: Physics and Applications" *Appl. Sci.* **2018**, *8*(4), 617; doi:10.3390/app8040617 (IF2.7; Q2).

A4. **V. P. Drachev**, A. V. Kildishev, J. D. Borneman, K-P. Chen, V. M. Shalaev, K. Yamnitskiy, R. A. Norwood, N. Peyghambarian, S. R. Marder, L. A. Padilha, S. Webster, T. R. Ensley, D. J. Hagan, and E. W. Van Stryland, Engineered nonlinear materials using gold nanoantenna array, **Scientific Reports 8**: 780 (2018). (IF 4.38; Q1)

A5. V.C. de Silva, P. Nyga, **V.P. Drachev**, Optimization and photomodification of extremely broadband optical response of plasmonic core-shell obscurants, **Journal of colloid and interface science** 484, 116-124 (2016). (IF 8.128; Q1)

A6. De Silva, Vashista C.; Nyga, Piotr; **Drachev, Vladimir P.** "Scattering suppression in epsilon-near-zero plasmonic fractal shells" **Optical Materials Express 5**(11), 2491-2500 NOV 1 (2015). (IF 3.064; Q1)

A7. **V. P. Drachev**, V. A. Podolskiy, and A. V. Kildishev, "Hyperbolic metamaterials: new physics behind a classical problem," **Optics Express** 21(12), 15048–15064 (2013). Highlighted in **Advances in Engineering** (https://advanceseng.com features breaking research judged by AE's advisory team). (IF 3.894; Q1)

A8. S. Ishii, A. V. Kildishev, E. Narimanov, V. M. Shalaev, and **V. P. Drachev,** "Subwavelength diffraction pattern from volume plasmon polariton in a hyperbolic medium," **Laser Photonics Review** (original paper) **7**(2), 265–271 (2013) (2013)./**DOI** 10.1002/lpor.201200095. (IF 10.66; Q1)

A9. J. Kim, **V. P. Drachev**, Z. Jacob, G. V. Naik, A. Boltasseva, E. E. Narimanov, and V. M. Shalaev, "Improving the radiative decay rate for dye molecules with hyperbolic metamaterials," **Optics Express** 20 (7), 8100-8116 (2012). (IF 3.894; Q1)

A10. S. Ishii, A.V. Kildishev, V.M. Shalaev, and **V.P. Drachev**, "Controlling the wave focal structure of metallic nanoslit lenses with liquid crystals" **Laser Physics Letters** 8(11), 828-832 (2011) / DOI 10.1002/lapl.201110077 (IF 2.328; Q1)

A11. A.V. Kildishev, J. D. Borneman, X. Ni, V. M. Shalaev, and **V. P. Drachev**, "Bianisotropic Effective Parameters of Optical Metamagnetics and Negative-IndexMaterials," (Invited paper) **Proceedings of the IEEE**, v. PP issue 99, 1-10 (2011) (IF 10.69; Q1)

A12. Kildishev, A.V.; Borneman, J.D.; Chen, K.-P.; **Drachev, V.P**. "Numerical Modeling of Plasmonic Nanoantennas with Realistic 3D Roughness and Distortion." **Sensors** 2011, *11*, 7178-7187. (IF 3.576; Q2)

A13. Mark D. Thoreson, Jieran Fang, Alexander V. Kildishev, Ludmila J. Prokopeva, Piotr Nyga, Uday K. Chettiar, Vladimir M. Shalaev and **Vladimir P. Drachev**, "Fabrication and realistic modeling of three-dimensional metal-dielectric composites", **J. Nanophoton**. 5, 051513 (May 23, 2011); doi:10.1117/1.3590208 (IF 1.415; Q1)

A14. S. Ishii, A. V. Kildishev, V. M. Shalaev, K.-P. Chen, and **V. P. Drachev**, "Metal nanoslit lenses with polarization-selective design," **Optics Letters** 36, Issue 4, 451-453 (2011). (IF 3.776; Q1)

A15. S. Xiao, **V.P. Drachev**, A.V. Kildishev, H.-K. Yan, U.K. Chettiar, and V.M. Shalaev, "Loss-free and active optical negative-index metamaterials," **Nature** 466, 735-738 (2010). (IF 42.78; Q1)

A16. K.P. Chen, **V.P. Drachev**, J.D. Borneman, A.V. Kildishev, and V.M. Shalaev, "Drude relaxation rate in grained gold nanoantennas," **Nano Letters** 10, 916-922 (2010). (IF 11.19; Q1)

A17. S. Xiao, U.K. Chettiar, A.V. Kildishev, **V.P. Drachev**, and V.M. Shalaev, "Yellow-light negative index metamaterials," **Optics Letters** 34, 3478 (2009). (IF 3.776; Q1)

A18. D. P. Brown, M. A. Walker, A. M. Urbas, A. V. Kildishevd, S. Xiao, and **V. P. Drachev,** "Direct measurement of group delay dispersion in metamagnetics for ultrafast pulse shaping," **Optics Express** 20(21), 23082-23087 (2012). (IF 3.894; Q1)

A19. R.M. Bakker, **V.P. Drachev**, Z. Liu, H.-K. Yuan, R.H. Pedersen, A. Boltasseva, J. Chen, J. Irudayaraj, A.V. Kildishev, and V.M. Shalaev, "Nanoantannae array-induced fluorescence enhancement and reduced lifetimes," **New Journal of Physics** 10, 125022 (2008) a special issue on Plasmonics.

A20. U.K. Chettiar, A.V. Kildishev, W. Cai, H.-K. Yuan, **V.P. Drachev**, and V.M. Shalaev, "Optical metamagnetism and negative index metamaterials," **MRS Bulletin** 33, 921-926 (2008). (IF 6.576; Q1)

A21. P. Nyga, **V.P. Drachev**, M.D. Thoreson, and V.M. Shalaev, "Mid-IR plasmonics and photomodification with Ag films," **Applied Physics B** 93, 59-68 (2008). (IF 2.07; Q1)

A22. J.-Y. Kim, **V.P. Drachev**, H.-K. Yuan, R.M. Bakker, V.M. Shalaev, "Imaging contrast under aperture tip- nanoantenna array interaction," **Applied Physics B** 93, 189-198 (2008). DOI 10.1007/s00340-008-3155-7. (IF 2.07; Q1)

A23. **V. P. Drachev**, U. K. Chettiar, A. V. Kildishev, W. Cai, H.-K. Yuan,, and V. M. Shalaev, "The Ag dielectric function in plasmonic metamaterials," **Optics Express** 16, 1186-1195 (2008). (IF 3.894; Q1)

A24. W**.** Cai, U**.** K. Chettiar, H**.**-K**.** Yuan, V**.** C. de Silva, A**.** V. Kildishev, **V. P. Drachev**, and V**.** M. Shalaev, "Metamagnetics with Rainbow Colors," **Optics Express** 15, 3333 (2007). (IF 3.894; Q1)

A25. U. K. Chettiar, A. V. Kildishev, H.-K. Yuan, W. Cai, S. Xiao, **V. P. Drachev**, and V. M. Shalaev, "Dual-Band Negative Index Metamaterial: Double-Negative at 813 nm and Single-Negative at 772 nm," **Optics Letters**, 32, 1671 (2007). (IF 3.776; Q1)

A26. H.-K. Yuan, U. K. Chettiar, W. Cai, A. V. Kildishev, A. Boltasseva, **V. P. Drachev**, and V. M. Shalaev, "A negative permeability material at red light," **Optics Express** 15, 1076-1083 (2007). (IF 3.894; Q1)

A27. T. Klar, A. V. Kildishev, **V. P. Drachev** and V. M. Shalaev, "Negative-index metamaterials: going optical," **IEEE J. of Selected Topics in Quant. Electronics** invited paper, 12, 1106-1115 (2006). (IF 4.9; Q1)

A28. V. M. Shalaev, W. Cai, U. Chettiar, H.-K. Yuan, A. K. Sarychev, **V. P. Drachev** , and A. V. Kildishev, "Negative index of refraction in optical metamaterials," **Optics Letters** 30, 3356 (2005). (IF 3.776; Q1)

A29. **V. P. Drachev,** W. Cai, U. Chettiar, H.-K. Yuan, A. K. Sarychev, A. V. Kildishev, and V. M. Shalaev, "Experimental verification of an optical negative-index material," **Laser Phys. Lett.** 3, 49-55 (2006) / **DOI** 10.1002/lapl.200510062 (2005). (IF 2.328; Q2)

A30. R. M. Bakker, **V. P. Drachev**, H.-K. Yuan, and V. M. Shalaev, "Enhanced Transmission in Near-Field Imaging of Layered Plasmonic Structures," **Optics Express** 12, 3701 (2004). (IF 3.894; Q1)

A31. **V. P. Drachev**, A. K. Buin, H. Nakotte, and V. M. Shalaev, "Size Dependent $\chi^{(3)}$ for Conduction Electrons in Ag Nanoparticles," **Nano Letters** 4, 1535 (2004). (IF 11.19; Q1)

A32. **V. P. Drachev**, E. N. Khaliullin, W. Kim, F. Alzoubi, S. G. Rautian, V. P. Safonov, R. A. Armstrong, and V. M. Shalaev, "Quantum size effect in two-photon excited luminescence from silver nanoparticles," **Phys. Rev. B** 69, 035318 (2004**).** (IF 4.036; Q1)

A33. **V. P. Drachev**, W. Kim, V. P. Safonov, V. A. Podolskiy, N. S. Zakovryazhin, V. M. Shalaev, and R. L. Armstrong, "Low-threshold lasing and broad-band multiphoton-excited light emission from Ag

aggregate-adsorbate complexes in microcavity," **J. of Modern Optics** 49, 645-662 (2002). (IF 1.6; Q2)

A34. **V. P. Drachev**, W. D. Bragg, V. A. Podolskyi, V. P. Safonov, W. Kim, Z. C. Ying, R. L. Armstrong, and V. M. Shalaev, "Large local optical activity in fractal aggregates of nanoparticles," **J. of Opt. Soc. Am. B** 18, 1896-1903 (2001). (IF 2.1; Q1)

A35. **V.P. Drache**v, S.V. Perminov, S.G.Rautian, and V.P. Safonov, "Giant nonlinear optical activity in aggregated silver nanocomposites," **JETP Letters** 68, 651-656 (1998). (IF 0.931; Q2)

B. INVITED CONFERENCE TALKS:

B1. **Drachev V.P.,** Spectroscopy of nanomaterials and metamaterials enhanced by plasmons, Russian Conference on fiber optics, Perm, Russia, October 8-11, 2019. (Invited)

B2. **Drachev V.P**., Plasmonics of nanoparticles with spin-polarization, XIII International Workshop on Quantum Optics, Vladimir, Russia, September 9-13, 2019. (Invited)

B3. **V. P. Drachev**, H. Bhatta, A. Aliev, "Spin-polarized plasmonics" META 2019, Lisbon - Portugal, July 22-26, 2019. (Invited)

B4. **V. P. Drachev**, H. Bhatta, A. Aliev, "Spin-polarized plasmonics: High Quality Plasmon Resonance in the Deep-UV," EMN Meeting on Nanoparticles 2019, Prague, June 10-14, 2019. (Invited)

B5. **V.P. Drachev**, G.I. Nazarikov, I.A. Pshenichnyuk, S.S. Kosolobov, "Si-based integrated microwave-photonics," International Symposium Flamn-19 Fundamentals of Laser Assisted Micro- & Nanotechnologies, June 30 - July 4, 2019, St. Petersburg, Russia. (Invited)

B6. **В.П. Драчев**, Спектроскопия биомолекул и метаматериалов усиленная плазмонными наноструктурами, Всеросийская Научная Конференция «Современные проблемы оптики и спектроскопии», Институт Спектроскопии, Москва, Троицк, 28-29 ноября 2018. (приглащенный)

B7. **Drachev V.P.,** Spectroscopy of biomolecules and metamaterials enhanced by plasmonic nanostructures, Russian Scientific Conference "Contemporary optics and spectroscopy," Institute of Spectroscopy, Russian Academy of Sciences, Moscow-Troitsk, November 28-29, 2018 (delivered in Russian). (Invited)

B8. **В. П. Драчёв**, Университет Северного Техаса (США); Сколковский институт науки и технологий, Плазмоника для радифотоники, XX Международная научно-техническая конференция «Проблемы Техники и Технологии Телекоммуникаций» ПТиТТ-2018, 20-21 ноября 2018, Уфа, Россия. (приглашенная лекция)

B9. **Drachev V.P.,** Plasmonics for microwave photonics, XX International Conference on "Problems on Techniques and Technology of Telecommunications." (Invited)

B10. **Драчев В.П.**, «Особенности плазмоники в наноструктурах со спиновой поляризацией и радиофотонике», Научная сессии отделения нанотехнологий и информационных технологий (ОНИТ) РАН, Нанофотоника в Информатике и Приборостроении, 15-16 ноября, 2018, Сколковский институт науки и технологий, Москва, Россия.

B11. **Drachev V.P.,** Advanced plasmonics for nanostructures with spin polarization and radio-photonics, Scientific session of Division on nanotechnology and information technology Russian Academy of Sciences "Nanophotonics for Information and Instrumentation," November 15-16, 2018, Skolkovo Institute of Sceince and Technology, Moscow, Russia. (Invited)

B12. **V.P. Drachev**, Plasmon coupled super- and sub- radiance from dye shells, 3rd International Conference on Metamaterials and Nanophotonics METANANO 2018, Sochi, Russia, 17-21 September, 2018. (Invited)

B13. **В.П. Драчев**, Плазмоника со спиновой поляризацией// Материалы семинара, 8-й Российский семинар по волоконным лазерам. (3-7 сентября 2018г., г. Новосибирск), 88-89 (2018). (Приглашенный)

B14. Drachev V.P., Spin-polarized plasmonics, Russian seminar on fiber lasers. Novosibirsk, Russia, September 3-7, 2018. Materials pp.88-89. (Invited)

B15. **V.P. Drachev**, V.C. de Silva, P. Nyga, Plasmonic fractal shells for drug delivery: broadband response, synthesis, and laser release, 18th International Conference on Laser Optics, St. Petersburg, Russia, 4-8 June, 2018. Invited talk.

B16. V.P.Drachev, Surface-Enhanced Raman Scattering of proteins, Skolkovo Institute of Science and Technology, University of North Texas, Department of Physics, Denton, TX, USA. Russian Conference on Combination (Raman) Scattering – 90 years of research. (Invited)

B17. **V.P. Drachev**, Nonlinear metamaterials, Scientific School for young researchers and students "Nonlinear Photonics," Perm, Russia, October 4-6, (2017). Invited Lecturer.

B18. H. Bhatta, A. Aliev, and **V. P. Drachev**, Spin-polarized plasmons in magnetic nanoparticles, Conference on Solitons, Collapses, and Turbulence, Chernogolovka, Russia, May 21-25 (2017). Invited.

B19. H. Bhatta, A. Aliev, and **V. P. Drachev**, New type of localized plasmons specific for spin-polarized magnetic nanoparticles, Conference on Quantum Nanophotonics, Benasque, Spain Feb 26-March 3 (2017). Invited.

B20. V. P. Drachev, D. Lyvers, "Life time and photon statistics of a single dye molecule near hyperbolic metamaterials," Conference Days of Diffraction, Workshop on Metamaterials; St.Petersburg, Russia, May 30-June 3, 2014 (Invited talk).

B21. **V.P.Drachev**, A. Krokhin, S.Ishii, A.V.Kildishev, "Hyperbolic metamaterials for nanophotonics," Conference on metamaterials, plasmonics, and photonic crystals META14, Singapore, May 20-23, 2014 (invited).

B22. **V.P.Drachev**, S.Ishii, A.V.Kildishev, "Tunable metamaterials with resonance and focusing properties," Conference on metamaterials, plasmonics, and photonic crystals META14, Singapore, May 20-23, 2014 (Invited talk).

B23. **V. P. Drachev**, D. Lyvers, "Nanophotonics with hyperbolic metamaterials," Conference on Fiber Lasers, Novosibirsk, Russia, April 14-18, 2014 (Invited talk).

B24. **V.P. Drachev**, K.Lee, J.P. Irudayaraj, "Spectroscopy of site specific DNA assembled plasmonic networks on cell surfaces," SPIE Optics and Photonics, Biosensing and Nanomedicine, San Diego, CA, USA, August 25-29, 2013 (invited).

B25. **Drachev V.P**., "Control of dye luminescence and nanolithography with hyperbolic metamaterials," Basic Problems of Optics, St Petersburg, Russia, October 15-19, 2012. (Invited talk).

B26. **V.P.Drachev** "Hybrid plasmonic metamaterials," Conference on metamaterials, plasmonics, and photonic crystals META12, Paris, France, April 19-22, 2012 (**Invited talk**).

B27. S.Ishii, A.V.Kildishev, V.M.Shalaev, E.E.Narimanov, and **V.P.Drachev** "Plasmonic lenses and subwavelength diffraction in hyperbolic media," Conference on metamaterials, plasmonics, and photonic crystals META12, Paris, France, April 19-22, 2012 (**Invited talk**).

B28. A. V. Kildishev, L. J. Prokopeva, D. P. Brown, A. M. Urbas, and **V.P.Drachev,** "Multiphysics of optical metamaterials: time-domain modeling," Conference on Advanced Electromagnetic Simulations AES12, Paris, France, April 16-18, 2012 (**Invited talk**).

B29. **V.P. Drachev** "Loss-free optical nanomaterials," Conference on Fiber Lasers, Novosibirsk, Russia, March 24-27, 2012 (**Invited talk**).

B30. **V.P. Drachev** "Plasmonics for bio-sensing and metamaterials" III International School and Conference on Photonics, Belgrade, Serbia August 27-September 2, 2011 **(Keynote lecture)**

B31. **V.P. Drachev**, A.V.Kildishev, W. Cai, U.K. Chettiar, S. Xiao, X. Ni, L. J. Prokopeva, E.E.Narimanov, V.M.Shalaev, "Transformation optics with metamaterials," Conference Days of Diffraction, Metamaterials workshop; St.Petersburg, Russia, May 30-June 3, 2011 **(Invited talk)**

B32. **V. P. Drachev,** Kyuwan Lee, and Joseph Irudayaraj, "Gold nanopaticles from nanoantennas to networks: fundamentals and applications," Conference Days of Diffraction, Metamaterials workshop; St.Petersburg, Russia, May 30-June 3, 2011 **(Invited talk)**

B33. **V.P. Drachev**, K.Lee, J. Irudayaraj, "Single-cell optical sensing with DNA-assembled gold nanoparticles," Interanational Conference on Coherent and Nonlinear Optics and Laser Applications and Technologies, August 23-26, 2010 Kazan, Russia **(Invited talk).**

B34. **V.P. Drachev**, P. Nyga, U.Chettiar, M. Thoreson, A.V. Kildisshev, V.M. Shalaev, "Simulation of semicontinuous films ," SPIE Plasmonics, San Diego, 1-5 Aug (2010). (**Invited talk**).

B35. **V.P. Drachev**, V. de Silva, P. Nyga, V.M. Shalaev, "Scattering cancellation with plasmonic shells," SPIE Plasmonics, San Diego, 2-6 Aug (2009). (**Invited talk**).

B36. **V. P. Drachev**, U. K. Chettiar, H. Yuan, W. Cai, A. V. Kildishev, V.M. Shalaev, Purdue Univ. Metamaterials with negative magnetism and refractive index for the visible range, ***(Invited Paper),*** Progress in Electromagnetics Research Symposium (PIERS), Hangzhou, China, March 24-28, 2008.

B37. **V. P. Drachev**, U. K. Chettiar, H. Yuan, W. Cai, A. V. Kildishev, V.M. Shalaev, Purdue Univ. Size effects in plasmonic metamaterials for the visible range, ***(Invited Paper),*** SPIE Conference on Optics and Photonics, San Diego, California, USA, August 28-30, 2007

B38. **V. P. Drachev**, U. K. Chettiar, H.-K.Yuan, W. Cai, M. D.Thoreson, A.V. Kildishev, and V. M. Shalaev, Real Metamaterials (**Invited**), International Conference on Coherent and Nonlinear Optics (ICONO), Conference on Lasers, Applications, and Technologies (LAT), Minsk, Belarus, May 28–June 1, 2007.

B39. **V. P. Drachev**, M. D. Thoreson, V. Nashine, M. Narasimhan, V. J. Davisson, V.M. Shalaev, SERS of proteins at monolayer density with adaptive plasmonic nanostructures, Pittcon 2006 (**invited**).

B40. **V. P. Drachev**, M. Thoreson, V. C. Nashine, M. Narasimhan, V. J. Davisson, D. Ben-Amotz, V. M. Shalaev, "Surface enhanced Raman Scattering of biomolecules with adaptive nanostructures", The third international conference on advanced vibrational spectroscopy (ICAVS-3), August 14-19, 2005, Delavan, Wisconsin, USA.(**Invited**)

B41. **V. P. Drachev**, "Optical metamaterials with negative refractive index: experiment", Joint Conference on Information Sciences, PNC, Workshop on Negative Index Media, July 21-22, 2005 (**invited talk**).

B42. **V. P. Drachev**, M. Thoreson, V. M. Shalaev, "Protein sensing with plasmonic nanostructures", International Conference on coherent and nonlinear Optics (ICONO), May 11-15, 2005 (**Invited talk**).

B43. **V.P. Drachev**, Optical nonlinearities in metal nanostructures, SIAM Conference on Nonlinear Waves and Coherent Structures, Orlando, FL, October 2-5, 2004 (**invited**).

B44. **V. P. Drachev**, Spectroscopy of metal quantum dots, SIAM (Society of Industrial and Applied Mathematics) annual meeting, Portland, OR, July 12-16, 2004 (**invited**)

B45. **V. P. Drachev**, M. Thoreson, E. Khaliullin, A. K. Sarychev, D. Zhang, D. Ben-Amotz, and V. M. Shalaev, "Semicontinuous silver films for protein sensing with SERS", SPIE annual meeting, 3-4 August 2003, San Diego, CA (**invited talk**).

C. INVITED LECTURES:

C1. V.P. Drachev, "Quantum size effect and optical activity in plasmonic nanomaterials"- Novosibirsk, Russia, Institute of Automation and Electrometry Russian Academy of Sciences, November 2003.

C2. V.P. Drachev, "Optics and spectroscopy of metal quantum dots and nanostructures"-Norfolk State University, Norfolk, April 2004.

C3. V.P. Drachev, "Plasmonic nanostructures towards negative index materials and biosensing"- Aston University, Birmingham, UK, December 2005

C4. V.P. Drachev, "Plasmonic metamaterials with negative refractive index"- The University of Arizona, College of Optics, Tucson, April 26, 2007.

C5. V.P. Drachev, "Ag dielectric function in plasmonic nanostructures for biosensing and metamaterials"- Purdue University, Department of Chemistry, Physical Chemistry Seminar, October 17, 2007.

C6. "Plasmonic nanostructures for biosensing and negative index materials"- Russian Academy of Sciences, Institute for Theoretical and Applied Electromagnetics, Moscow, November 2, 2007.

C7. V.P. Drachev, "Plasmonic nanostructures for metamaterials and luminescence control," Wave Function Engineering 2009, Los Alamos, NM 25-27 Feb (2009).

C8. V.P. Drachev, "Plasmonic optical metamaterials," AFRL Workshop on Metamaterials, Dayton, OH, Oct 9 (2009).

C9. V.P. Drachev, "Recent progress in plasmonic metamaterials," Moscow Institute for Physics and Technology, International School of Optics for young scientists, October 16, (2009).

C10. V.P. Drachev, "Plasmonic applications for biosensing and optical metamaterials" Russian Academy of Sciences, Institute for Physics of Solid State, Chernogolovka, October 19, 2009.

C11. V.P. Drachev, "Surface-enhanced Raman scattering and plasmonic metamaterials," Moscow Institute for Physics and Technology, Dolgoprudnyi, October 21, (2009).

C12 V.P. Drachev "Active plasmonics for optical metamaterials with negative refractive index"- The University of Arizona, Department of Physics, Tucson, February 12, 2010.

C13. V.P. Drachev "Nanoplasmonics for active metamaterials and biosensing," University of North Texas, Department of Physics, Denton, TX, February 22, 2011.

C14. V.P. Drachev "Nanoplasmonics for active metamaterials and biosensing," University of Texas-Dallas, Institute for nanotechnology, Department of Physics, Dallas, TX, February 23, 2011.

C15. V.P. Drachev "Losses in nanostructured metals and active metamaterials," Southeastern Methodist University, Department of Mathematics, Dallas, TX, February 24, 2011.

C16. V.P. Drachev "Nanoplasmonics in metamaterial- and bio-applications" Workshop on plasmonics and Metamaterials, Buffalo NY, May 16-17 2011.

C17. V.P. Drachev "Plasmonic nanophotonics: the fundamentals behind applications," University of North Texas, Department of Physics, Denton, TX, February 7, 2012.

C18. V.P. Drachev “Luminescence and nonlinear optics of hybrid plasmonic nanomaterials” Workshop on Linear and Nonlinear Optical Interactions in Metamaterials and Plasmonic Nanostructures, Huntsville AL (USA), June 21-22 2012.
C19. Drachev V.P. “Control of luminescence and nonlinear response of dyes with plasmonic nanomaterials,” UT Dallas, Sep 26, 2012.
C20. Drachev V.P. “Optical metamaterials based on plasmonic nanostructures,” St Petersburg State University, Russia, October 16, 2012.
C21. Drachev V.P. “Nanoplasmonics for hybrid metamaterials and biosensing,” SUNY at Buffalo, Buffalo, NY, Feb 7, 2014.
C22. Drachev V.P. "Spectroscopy and Photonics of Plasmonic Metamaterials," SkolTech, Skolkovo, Aug. 6, 2015.
C23. Drachev V.P. L.D. Landau Institute of Theoretical Physics, Chernogolovka, Russia, May 20, 2016.
C24. Drachev V.P. Plasmonic nanostructures for metamaterials and spectroscopy, Institute of Spectroscopy, Russian Academy of Sciences, Troitsk, Russia, May 18, 2017.
C25. Drachev V.P. Plasmonics for optical metamaterials and biosensing, Texas A&M University, Commerce, TX, USA Feb 1, 2018.
C26. Drachev V.P., Photonics and its applications, Public lecture for faculty and students, Ufa State Aviation Technical University, November 19th 2018, Ufa, Russia (lecture delivered in Russian).
C27. Drachev V.P., Plasmonics News: recent developments at UNT, University of North Texas, Physics Colloquium, February 26th, 2019.
C27. Drachev V.P., Plasmonic nanomaterials for biomedical applications, University of Texas Medical Branch, Houston March 1, 2019.
C28. Drachev V.P., Plasmons in magnetic nanoparticles with spin polarization, A.A. Baikov Institute of Metallurgy and Material Science, Russian Academy of Sciences, Moscow. November 18th, 2019.
C29. Drachev V.P., Spin-polarized plasmonics: high quality plasmon resonance in the deep-UV, University of North Texas, Physics Colloquium, February 11th, 2020.

DISSERTATION DESCRIPTION

Chapter I. Dielectric function of noble metals in plasmonic nanostructures

(based on papers A2, A4, A12, A13, A16)

First chapter presents the results on important question for the permittivity of metals, which can be different from bulk materials due to the quantum-size effect, saturation of the local field enhancement at relatively high intensity. Ag permittivity in coupled strips is different from bulk and has been studied for strips of various dimensions and surface roughness. Arrays of such paired strips exhibit the properties of metamagnetics. The surface roughness does not affect the Ag dielectric function, although it does increase the loss at the plasmon resonances of the coupled strips. The size effect is significant for both polarizations of light, parallel and perpendicular to the strips with large A-parameter. A-parameter is introduced in the literature as a coefficient at the relaxation constant due to quantum-size effects.

I.1 Ag permittivity in coupled strips

Figure 1 collects the spectra of the imaginary part of the Ag dielectric function $\varepsilon_m''(\lambda,\alpha,\beta)$ for all five samples and both TM and TE polarizations. The data for the bulk dielectric function from two literature sources [22-23] are shown for comparison. The size dependence of the dielectric function is clearly seen here for both polarizations. We extracted the size-dependent term of the relaxation rate, $\gamma_{size} = \gamma(w) - \gamma_\infty = A V_F / w$, which can be presented (see dissertation) as a function of the inverse effective width of the strips, $w_{eff}^{-1} = 0.5(w_t^{-1} + w_b^{-1})$. The simulations with two widths, representing the top and bottom strips, and simulations with the dielectric function using an effective width for both strips show good correspondence. The calculated A-parameters for the two polarizations are $A_{\mathrm{TM}} \approx 4.2 \pm 0.3$ and $A_{\mathrm{TE}} \approx 2.3 \pm 0.3$.

One can see that ε_m'' for the three samples with similar widths show almost no differences, indicating that the roughness does not affect the dielectric function. However, the distorting effect of roughness on the geometry is exhibited by the differences in the absorption spectra and the strong difference in the retrieved permeabilities of the effective layer.

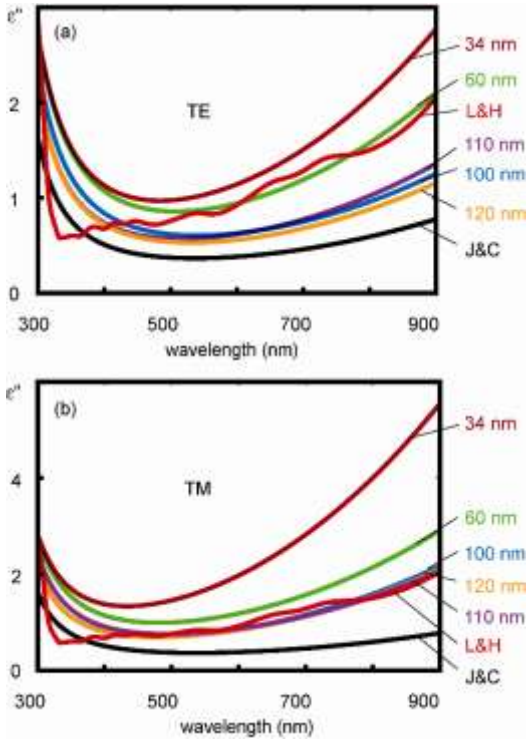

Figure 1: The experimental spectra of the imaginary part of the Ag dielectric function in the coupled strips for five samples (strip width is shown at the right for each sample) in comparison with the bulk dielectric function from two sources J&C, Ref. [22] and L&H, Ref. [23] for TE (a) and TM (b) polarizations.

The results of our experiments on the Ag dielectric function in coupled strips lead us to several important conclusions. First of all, the spectra of ε_m'' for the TE polarization (electric field parallel

to the strips) suggest good quality of the Ag crystal structure. Indeed, ε_m'' for samples with large widths are between the literature values from Johnson and Christy, and Lynch and Hunter [22-23] for bulk Ag carefully fabricated with subsequent polishing and annealing. As we mentioned above, a very probable reason for the diversity in the bulk Ag dielectric function is the term in the electron relaxation rate describing crystal defects and grain boundaries, ν_{ed}. The strips have a reasonable ε_m'' for the TE polarization, comparable with bulk, large-area films.

I.2 Drude Relaxation Rate in Grained Gold Nanoantennae

Section 1.2 presents effect of grain boundaries on the electron relaxation rate, which is significant even for large area noble metal films and especially for nanostructures. Optical spectroscopy and X-ray diffraction show substantial improvement of the plasmon resonance quality for the square type nanoantennae due to 1.8 times enlarged grain size after annealing and improved grained boundaries described by the electron reflection coefficient. The electron relaxation rate decreases by factor 3.2. It was shown also that the annealing may act in a negative way depending on the nanostructure shape.

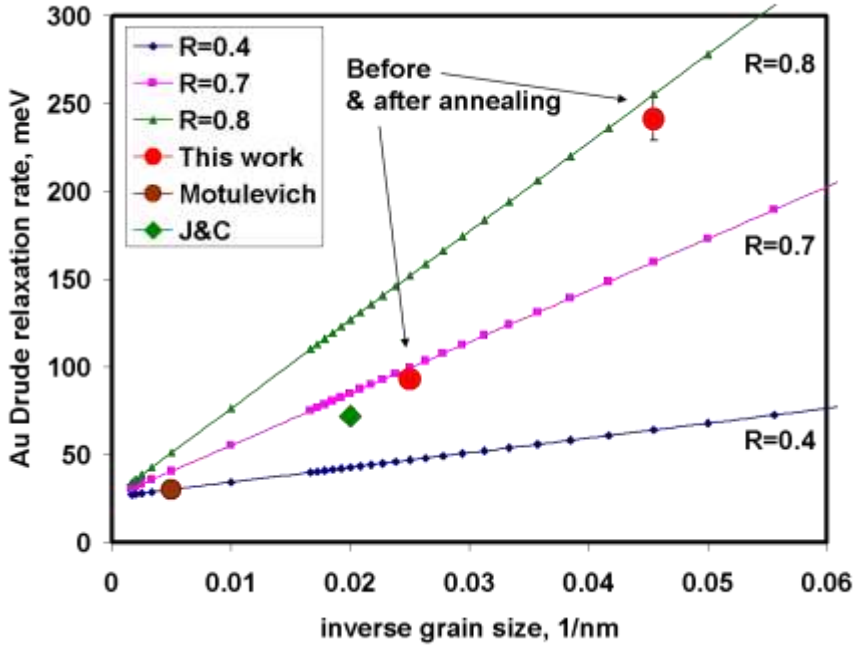

Figure 2: Au electron scattering rate in meV, Γg (Γ_0=26 meV) calculated with the model I2.5 at R=0.4, 0.7, and 0.8. The results for nanoantennae gold were plotted with red circles. The Motulevich [25] data for gold shown in brown circle, and green square is for Johnson and Christy result. The grain size is taken approximately film thickness, 50 nm in the J&C case.

The solution for the relaxation time can be approximated by simple linear dependence on the inverse grain size D^{-1} [24]:

$$\tau_g^{-1} = \tau_0^{-1} + \frac{1.37 \upsilon_F R}{D(1-R)}. \qquad \text{(I2.5)}$$

In this equation τ_0 is the relaxation time of infinite grain size, $\upsilon_F = 1.35 \times 10^6$ m/s is the Fermi velocity for Au. A choice of the reference relaxation rate for the infinite grain size requires special discussion. Careful consideration of possible sources shows that there are not so many measurements where grain size contribution was determined. The data obtained by Motulevich for gold films are supported by grain contribution in the resistance and grain size measurements [25]. It was determined as $R_{res}/R=\nu_{ed}/(\nu_{ep}+\nu_{ed})$, where residual resistance R_{res} was measured at 4.2K. The electron relaxation rate for infinite grain size is caused by electron-phonon collision rate $\Gamma_0=\Gamma_{ep}$=26 meV, and grain contribution Γ_{ed}=4 meV with grain size about 200 nm. Using the value $\tau = 2.7 \times 10^{-14} s$ (note that $\tau = 2.56 \times 10^{-14} s$ for optical measurements by Motulevich) as calculated from 295K resistivity data on pure bulk crystals and assuming that the conduction effective mass equals to free-electron mass. The grain boundary reflection coefficient, R is often taken to be 0.5 as the first approximation. One can see, however, from our data that the reflection coefficient can be different for the nanoantenna before and after annealing likely due to increased volume fraction of the grain boundaries and consequently the strength of the scattering potentials. We should note that the difference in barrier reflection coefficient between 0.7 and 0.8 makes a big difference in the relaxation rate for the same grain size, which is about 100 meV at 22 nm and much larger the experimental error in the relaxation rate measurements.

I.3 Size dependent $\chi^{(3)}$ for conduction electrons in Ag nanoparticles

(based on papers A30-A35)

Section 1.3 presents our theoretical analysis of the third-order susceptibility ($\chi^{(3)}$) for Ag dielectric composite reveals a critical role of saturation of optical transitions between discrete states of conduction electrons in metal quantum dots. We use Rautian's approach [26]. The calculated size dependence of the $\chi^{(3)}$ for Ag nanoparticles is in a good agreement with published experimental results [27], in contrast to the commonly used theoretical approach [28]. Saturation effects are responsible for a decrease of the local field enhancement factor that is of particular importance for surface-enhanced phenomena, such as Raman scattering and nonlinear optical responses.

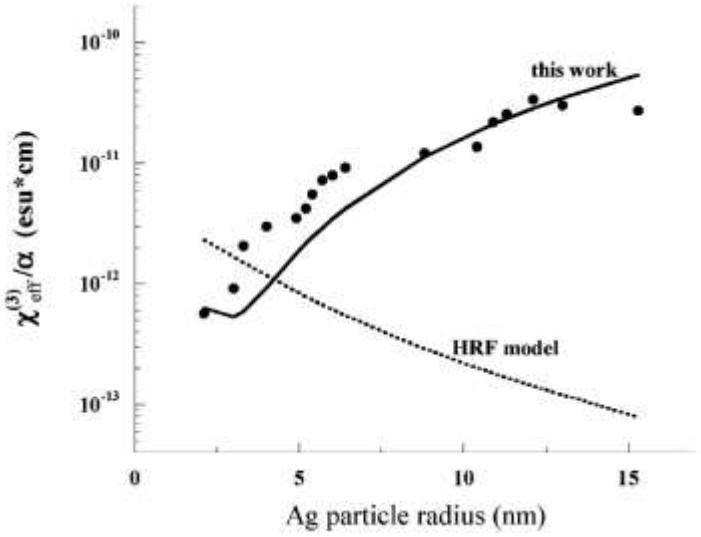

Figure 3: Comparison of the dependence of $\chi^{(3)}_{eff}/\alpha$ on Ag particle size using the theoretical approach discussed in this work (solid line) with the experimentally determined values (symbols) from Uchida et al. [27] and the one by Hache, Ricard and Flytzanis (HRF) [28] (dashed line). Note that a logarithmic *y*-axis has been used for clarity.

We were able to reproduce the experimentally observed size dependence on $\frac{\chi^{(3)}_{eff}}{\alpha}$ in Fig.3 using the theoretical treatment proposed by Rautian [26]. This behavior cannot be explained by the Hache, Ricard and Flytzanis (HRF) approach [28], widely used though for the description of experimental results in metal particle composite systems. It is important to note that our treatment is only dealing with contribution from conduction electrons, and it does not address interband transitions. Furthermore, our studies emphasize the importance of saturation effects for the local field enhancement factor, which strongly affects nonlinear processes and SERS. Our results suggest the saturation of optical transitions in metal nanostructure as the probable reason for the decrease in SERS enhancement. Therefore, the saturation will be especially important when using high-intensity laser light typical for pulsed fs and ps lasers.

Chapter II. New mechanism of plasmons specific for spin-polarized nanoparticles

(based on papers A1)

Second chapter covers peculiarities of localized plasmons in the case of spin polarized magnetic nanoparticles. Our experiments on Co nanoparticles with a single-domain crystal structure show that they support a plasmon resonance at approximately 280 nm with better resonance quality than gold nanoparticle resonance in the visible. Magnetic nature of the nanoparticles suggests a new type of these plasmons. The exchange interaction of electrons splits the energy bands between spin-up electrons and spin-down electrons Fig.4 (insert).

Electron scattering without spin flip makes possible a coexistence of two independent channels of conductivity as well as two independent plasmons in the same nanoparticle with very different electron relaxation. Indeed, the density of empty states in a partially populated d-band is high, resulting in a large relaxation rate of the spin-down conduction electrons and consequently in low quality of the plasmon resonance. In contrast, the majority electrons with a completely filled d-band do not provide final states for the scattering processes of the conduction spin-up electrons, therefore supporting a high quality plasmon resonance. The scattering without spin flip is required to keep these two plasmons independent.

High quality plasmon resonance in absorption is proven below to be the property of isolated Co nanoparticles. Indeed, we observe a complete suppression of sharp plasmon resonance for aggregated Co nanoparticles, probably due to the interparticle interaction inducing a spin-flip electron scattering at the particle surface. This behavior is reversible, i.e., the sharp resonance is completely restored for separated nanoparticles after sonication, as shown below. Note that the

absence of cobalt oxide shell, which could introduce an antiferromagnetic response, is controlled with the low temperature SQUID measurements.

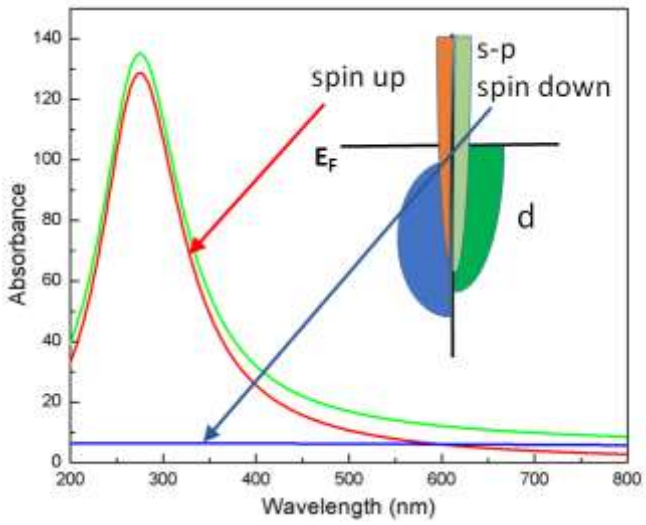

Figure 4: Two plasmon model for Co nanoparticles absorbance. ω_{sp} is taken to be 280 nm from experiment. Green is the sum of red (spin up) and blue (spin down). Insert: a cartoon of the projected density of states typical for Co.

The ab-initio simulations of the relaxation constants performed for the giant magnetoresistance show a large difference for spin-up and spin-down electrons [29,30]. Susceptibility of Co nanoparticles can be expressed as a sum of two terms coming from two independent groups of electrons. Thus, the total polarizability is given by:

$$\alpha = r^3(\chi_\uparrow + \chi_\downarrow) = r^3\left(\frac{1}{X_\uparrow + i\delta_\uparrow} + \frac{1}{X_\downarrow + i\delta_\downarrow}\right). \qquad \text{(II.1)}$$

Here we use the spectral representation of the Drude-Sommerfield model [31,32].

$$\chi_i = \frac{\varepsilon_h - \varepsilon_{mi}}{2\varepsilon_h + \varepsilon_{mi}} = \frac{1}{X_i + i\delta_i}, \quad \varepsilon_{mi} = \varepsilon_{0i} - \frac{\omega_p^2}{\omega(\omega + i2\Gamma)}, \varepsilon_h \approx \varepsilon_0, \quad \omega_{sp}^2 = \frac{\omega_p^2}{\varepsilon_0 + 2\varepsilon_h}, \qquad \text{(II.2)}$$

$$X_i = \frac{\omega_{sp}^2 - \omega^2}{\omega_{sp}^2}, \delta_i = \frac{\omega 2\Gamma_i}{\omega_{sp}^2}, \quad 2\Gamma_\uparrow = \upsilon_F/\lambda_\uparrow \text{ and } 2\Gamma_\downarrow = \upsilon_F/\lambda_\downarrow, \text{ where } \lambda_\uparrow = 12\,\text{nm}, \lambda_\downarrow = 0.6\,\text{nm},$$

Fermi velocity $\upsilon_F = 2.1\times10^5\,\text{m/s}$, thus $2\Gamma_\uparrow \approx 72.4\,\text{meV}$ and $2\Gamma_\downarrow \approx 1448\,\text{meV}$ [29,30]. Extinction cross-section is kImα. Thus, the absorption spectra should appear as a sharp resonance, due to spin-up electrons, plus a broad background coming from spin-down electrons (Fig. 4). Therefore, as soon as all possible electron scattering processes occur without spin-flip, meaning that two group of electrons are independent, one should expect sharp plasmon resonance. In particular, it

requires single domain nanoparticles, since inter-domain walls increase probability of spin flip electron scattering and thus two group of electrons are no longer independent.

To prove this concept, we perform experiments showing sharp plasmon resonance for isolated,

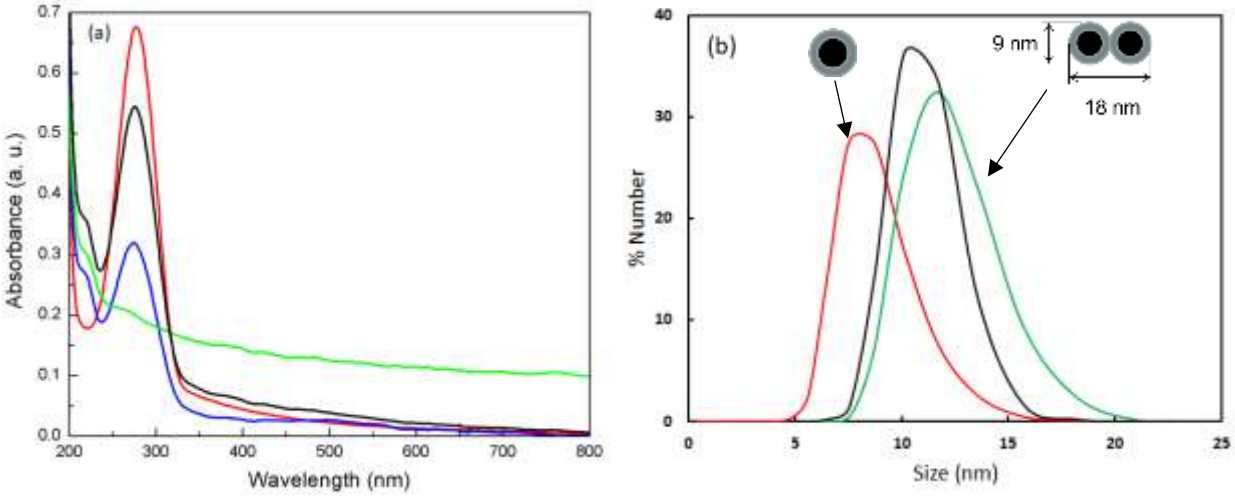

Figure 5. (a) Experimental absorbance of Co-NPs in hexane. As grown Co-NPs (red), after 1 hour sonication with external 130 mT DC magnetic field (blue), after 2.5 hours sonication with external 130 mT DC magnetic field (green, plasmon peak is demolished), no magnetic field and 1 hour sonication (black). (b) Co-NPs size distribution measured with dynamic light scattering (red)- as grown; (green) - 2.5 hours sonication with external 130 mT DC magnetic field; (black) after 1 hour sonication without magnetic field.

single-domain Co nanoparticles (Co NPs), but plasmon resonance disappears if small, two-three particles aggregates are formed. The magnetization measurements by SQUID system (dissertation) show superparamagnetic properties of the Co NPs at room temperature, which indicates the single-domain structure. The temperature dependence of the magnetization gives blocking temperature, which corresponds to the particle volume of this size. Below the blocking temperature field dependence of the magnetization has hysteresis behavior. The shift of the hysteresis loop cooled to 10 K at field +1 T and opposite shift for the sample cooled at -1 T allows to control the oxidation level of nanoparticles (see dissertation for details). All the results below correspond to the particles without an oxide shell. Figure 5 demonstrates remarkable resonance quality of the representative spectrum for Co NPs in hexane solution. The plasmon resonance quality is about the same as for gold nanoparticles, which have resonance in the green spectral range. Co-NPs are isolated due to surfactants, trioctylphosphine and oleic acid. Dynamic light scattering data show an average size close to the mean size from TEM images.

The following experiment illustrates interaction of Co nanoparticles separated by thin surfactant shell. To initiate aggregation, the 130 mT DC magnetic field together with sonication were applied to the Co NP hexane suspension in a quartz cuvette. After 1 hour of "aggregation" the dynamic light scattering and absorption spectra were collected. Figure 5a shows reduced plasmon peak (shown in blue). After 2.5 hours of sonication in magnetic field, the plasmon peak disappeared (shown in green). The dynamic light scattering shown in the Fig.5b gives increase in

the hydrodynamic particles size from 8.7 to 12-13 nm corresponding to small, two-three particles aggregates. It is remarkable that the following sonication, without external magnetic field, separates aggregated particles and the plasmon resonance is restored. Thus, this magnetic/sonication induced aggregation is a reversible process.

Chapter III. Optical metamaterials with magnetism and negative refractive index.

(based on papers A3,A11,A14,A15,A17-A21,A24-A29)

Third chapter discusses experimental demonstration of feasibility for optical negative index metamaterials. We start with comprehensive studies of a periodic array of gold nanorods pairs in section III.1 to demonstrate unique optical properties of this array near the plasmon resonance, high anisotropy of transmission and refractive index, high reflection below resonance frequency at about 10% of metal coverage, and a negative refractive index in the optical range above the plasmon resonance.

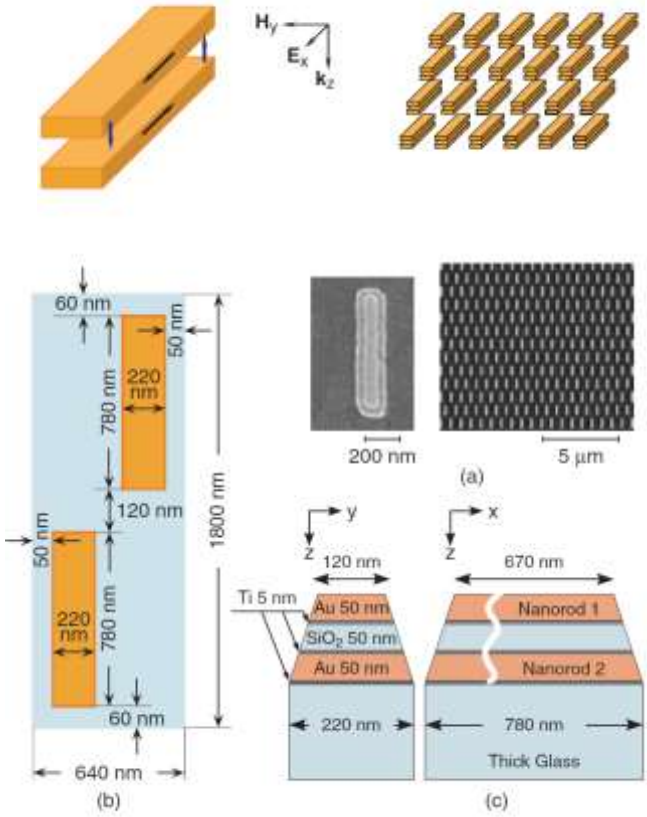

Figure 6. Pairs of parallel metal nanorods. (upper panel) A schematic for the array of nanorods and light polarization. (a) Field-emission SEM picture (top view) of a single pair of nanorods (left) and a fragment of 2 mm × 2 mm array of pairs of nanorods (right). (b) Sizes of the lower nanorods and their separations in the array, and (c) side-view cross-section schematics for one pair of nanorods on glass substrate.

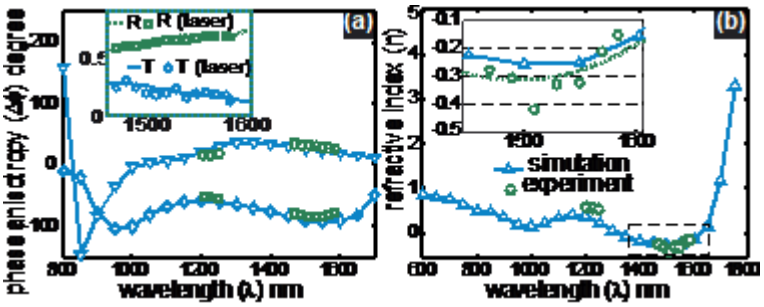

Fig. 7. (a) Phase anisotropy $\Delta\phi = \phi_{\parallel} - \phi_{\perp}$ for transmitted (◊ simulation and □ experiment) and reflected (▽ simulation and ○ experiment) light. The inset in (a) shows measured transmittance and reflectance magnitudes for the parallel polarization verified with laser measurements. (b) The real part of the refractive index restored from experimental data and compared to simulations. The inset depicts a zoomed view of the region of negative refraction; the dashed line represents the quadratic least-square fit for experimental data (○) and the solid line shows the simulated data (△).

A negative refractive index was obtained for the sample, containing array of nanorods fabricated directly on glass (Fig.6). In Fig. 7a we show the results of our phase measurements for the sample, which were performed with diode lasers and a tunable erbium laser. The detected phases are in excellent agreement with simulations. The inset depicts the measured transmittance and reflectance magnitudes (for the parallel polarization) verified with the erbium laser in the spectral range of interest where n is negative. Fig.7b exhibits n' obtained with the use of Eq. III.1. (n'' is not shown here.)

Following Ref. [33] where a single layer was considered, the complex index of refraction (n) of the nanorod layer on a substrate can be found from:

$$\cos nk\Delta = \frac{1 - r^2 + n_s t^2}{(n_s + 1)t + rt(n_s - 1)}, \qquad \text{(III.1)}$$

where n_s is the refractive index of substrate ($n_s = 1.48$ for our bare glass substrate).

Equation (III.1) provides the solution for retrieving the refractive index and impedance of a given thin layer of a passive material ($n'' > 0$ and $Z' > 0$, where $Z = Z' + iZ''$ is the impedance) with unknown parameters. Specifically, we obtain the impedance (not shown here) and the refractive index of the equivalent homogeneous layer with the same complex reflectance r and transmittance t as the actual array of nanorods. Such a homogeneous layer with equivalent n and Z gives the same far-field distribution outside the sample as the actual layer of metamaterial. Note that for a thin layer such retrieval can be performed unambiguously.

Simulations performed in our work suggest a relatively weak sensitivity of n' to variations in reflectance and transmittance amplitudes and its critical dependence on phases. The excellent agreement between calculated and measured phase shifts resulted in close values for the simulated and experimental values of n'. We note that the obtained absolute phase shift of -61º (see disseration) in the light transmittance at $\lambda = 1.5\,\mu m$ is well below the critical phase $-\phi_0 = -40^\circ$ at $1.5\,\mu\mathrm{m}$, so the phase criterion used above also predicts negative refraction in this case. The refractive index is negative between 1.3 μm and 1.6 μm, with $n' = -0.3 \pm 0.1$ at $\lambda = 1.5\,\mu m$. The spectral range of a negative n' is shifted with respect to the resonance providing a rather high transmittance of about 20%.

III.2 Metamagnetics using gratings

Section III2 presents optical magnetic metamaterials, which have been developed to demonstrate artificial magnetic response in the near infrared and across the entire visible spectrum.

We compare two samples with different roughness. Measurements of the root-mean square (RMS)

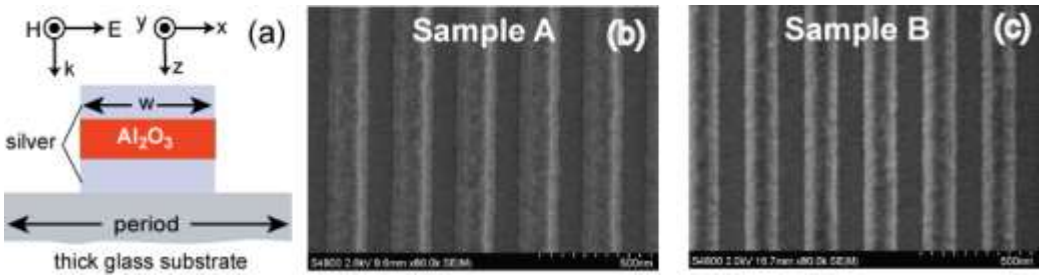

Figure 8. (a) Schematic of a pair of nanostrips, (b) SEM image of sample A, (c) SEM image of sample B.

value of surface roughness using a Veeco DI3100 atomic-force microscope (AFM) indicated that a slower deposition rate of silver (0.5 Å/s, Sample B) resulted in lower surface roughness than a faster deposition rate (~2Å/s, Sample A). Note that for a *typical* deposition procedure, the rate cannot be set lower than 2 Å/s, since the deposition of silver heats of the resist material and makes the lift-off process impossible. To cool down the resist, we performed a novel 4-step deposition process with 10-minute pauses between each deposition step. This new procedure allows the use of a slower deposition rate of about 0.5 Å/s in order to obtain a lower surface roughness while ensuring successful lift-off, providing an overall better quality sample. The vertical layer structure of the films from the ITO-coated glass was: Sample A, 10 nm alumina, 30 nm silver, 40 nm alumina, 30 nm silver, 10 nm alumina; Sample B, 10 nm alumina, 35 nm silver, 40 nm alumina, 35 nm silver, 10 nm alumina. A representative SEM image of the fabricated structure of Sample A is shown in Figure 8(b), while Sample B is shown in Figure 8(c). The images were taken using a Hitachi S-4800.

To test the fabricated samples, we measured transmission and reflection spectra of the samples with an ultra-stable tungsten lamp (B&W TEK BPS100). The spectral range of the lamp covers the entire visible and near-infrared optical band. A Glan-Taylor prism was placed at the output of the broadband lamp to select light with desired linear polarization. The signal transmitted (or reflected) from the sample was introduced into a spectrograph (Acton SpectraPro 300i) and eventually collected by a liquid-nitrogen cooled CCD-array detector. The transmission and reflection spectra were normalized to a bare substrate and a calibrated silver mirror, respectively. In the transverse electric (TE) regime the electric field of the incident light was linearly polarized parallel to the length of silver strips, while in the transverse magnetic (TM) mode the electric field was rotated 90 degrees relative to TE case. For example, Figures 9(a) and 9(b) show transmission and reflection spectra obtained from the optical measurements of Sample A and Sample B for TM polarizations at normal incidence along with the simulated results.

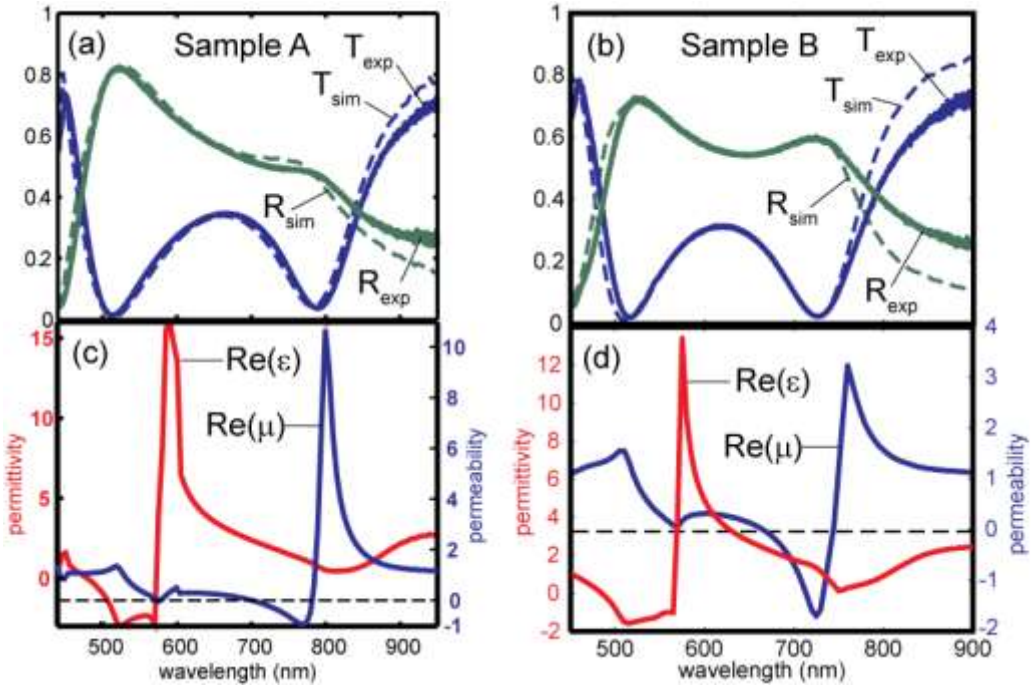

Figure 9. (a,b) Spectra of Sample A and Sample B respectively. Solid lines represent experimental data and dashed lines represent simulated data. T is transmittance and R is reflectance. (c,d) Real parts of retrieved effective permeability and permittivity for Sample A and Sample B respectively.

Figures 9(c) and 9(d) show the real parts of the retrieved effective permeability and permittivity for Samples A and B, respectively. Sample A and B show negative permeabilities of –1 and –1.7 at 770 nm and 725 nm respectively. In the TE polarization, both samples act like a dilute metal film without any resonant response.

III.3 Negative index materials based on cross-gratings

Metamaterials showing negative refractive index, also called *negative index materials* (NIM) have been demonstrated in the near infrared and at the border with the visible spectral range. Here we report the results of a sample that displays NIM behavior for red light at a wavelength of 710 nm. This is the shortest wavelength so far at which NIM behavior has been observed for the optical range. We also discuss the fabrication challenges and the impact of fabrication limitations, specifically surface roughness of the fabricated structures on the properties of the metamaterials.

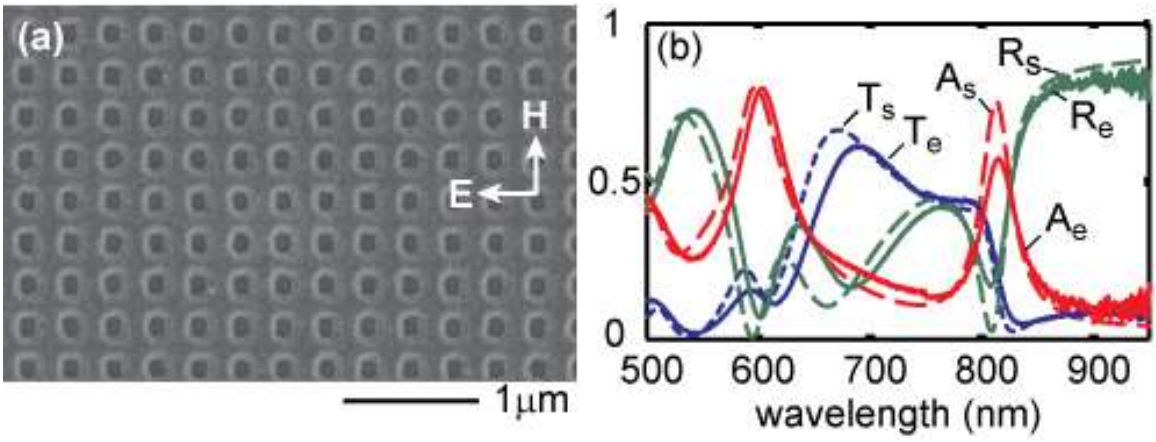

Figure 10. (a) FE-SEM image of the DN-NIM sample, (b) Experimental and simulated spectra of the DN-NIM sample. Solid lines represent experimental data and the dashed lines represent simulated data. T is transmittance, R is reflectance and A is absorbance.

The retrieved results for the sample are shown in Figure 11. The real part of the refractive index (n') and the figure of merit, the figure of merit (FOM = $-n'/n''$) are depicted in Figure 11 (a) (For the sake of clarity FOM is set to zero when $n' > 0$). The best FOM of 1.3 is obtained at a wavelength of 813 nm, where n' is about –1.0. The minimum value of the refractive index, $n' \approx -1.3$, is achieved at 820 nm, but with a lower FOM of 0.9. As indicated in Figure 11 (b), μ' is negative between 799 and 818 nm. This band is the dual-negative (DN)-NIM regime. In this wavelength range, ε' varies within the range of –1.2 ±0.1. The strongest magnetic response ($\mu' \approx -0.7$) is obtained at a wavelength of 813 nm, where $\varepsilon' \approx -1.1$. The same sample also demonstrates a SN-NIM response at the orthogonal polarization. In the orthogonal polarization the structure shows a maximum FOM of 0.7 at 772 nm with $n' \approx -1.0$.

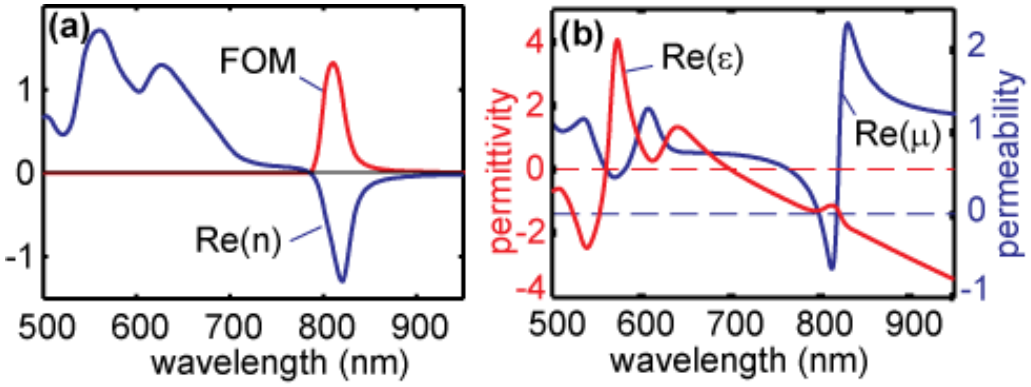

Figure 11. (a) Real part of refractive index and figure of merit (FOM) for the dual negative (DN)-NIM sample, (b) Real part of permittivity and permeability for the DN-NIM sample.

Section III.4 Optical negative index metamaterials with compensated losses

(based on A16.)

Optical NIMs are artificially tailored composites where a counterintuitive negative refractive index arises from the nanoscale "meta-atoms" designed into the material. These optical NIM building blocks typically require a plasmonic material such as silver or gold in addition to dielectric constituents. Losses inherent in these noble metals at optical frequencies plague the entire field of metamaterials and are one of the major restrictions preventing metamaterials from leaving the domain of academic research and entering industrial applications.

In earlier works, incorporating an active material has been suggested as a viable and effective method to minimize or eliminate loss in NIMs. However, in a NIM-based device the thickness of the active material must be kept necessarily small in order to preserve the negative refractive index. Therefore, the incorporation of gain in an optical NIM design is mired in difficulty, even though such an achievement would produce low- or no-loss optical NIMs for use in a large number of breakthrough applications.

We have overcome this limitation by an approach in which the active medium within the NIM gives rise to an effective gain much higher than its bulk counterpart. The large value of gain is achieved due to the local-field enhancement inherent to the plasmonic response of NIMs, providing a new direction for the compensation of losses in NIMs. In our experiments, the transmission through the optical NIM sample is amplified by pumping the active medium incorporated within the sample, and the structure is carefully designed to make the active medium experience the highest local field while simultaneously preserving the negative index property of the metamaterial. Our experimental results, along with our numerical simulations, directly demonstrate the first lossless and active NIM.

With a change in the refractive index accompanying the loss compensation, the impedance at the interface between the sample and air becomes mismatched, and thus the spectral reflection also

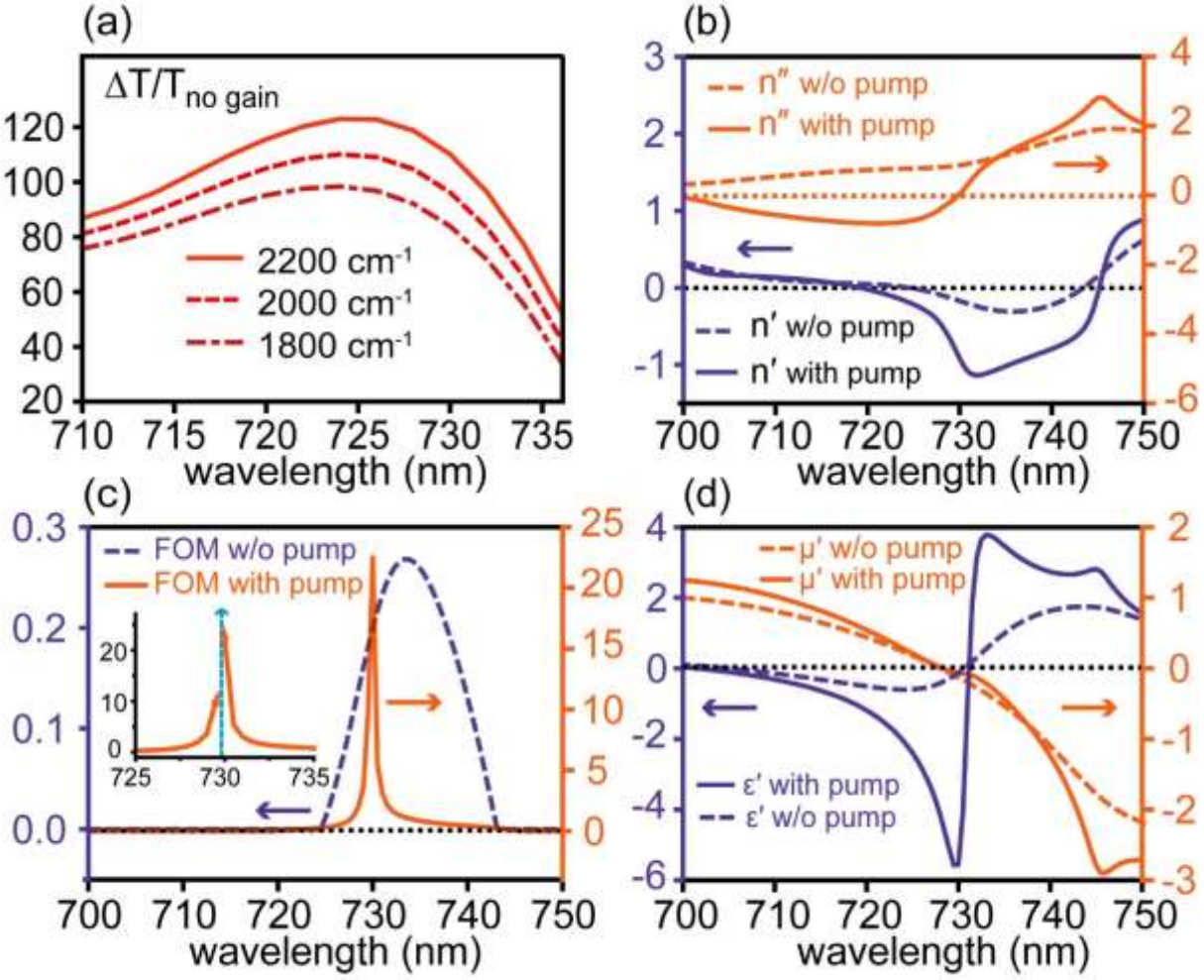

Figure 12. Simulation and retrieved parameters. (a) The simulated increase in transmission normalized to transmission without pump at three gain coefficients 1800, 2000, and 2200 cm^{-1}; (b) The retrieved effective refractive index $n = n' + i\,n''$ with and without gain; (c) The retrieved effective FOM with and without gain (the FOM is set to zero when the real part of the refractive index is positive); (d) The effective permittivity and permeability (real parts) with and without gain.

increases with gain, reaching 107.6% at 730 nm. The sum of the field intensities in transmission and reflection is nearly 1.23 times larger than the intensity of the incident beam at this wavelength. This confirms that the incident light is indeed amplified in the sample so that the absorbance A is negative and the sample is active.

According to Fig. 12(a), the NIM remains active within a spectral range between 722 nm and 738 nm, while the refractive index is negative in a broader range between 720 nm and 760 nm.

The effective refractive index and FOM were retrieved from the simulated spectra and are shown in Fig. 12. The real part of the refractive index *n*' becomes more negative after gain is applied, and the imaginary part *n*" also drops significantly near the resonance. At 737 nm, n' changes with the addition of gain from –0.66 to –1.017, while *n*" drops from 0.66 to 0.039 (see Fig. 12(b)). This corresponds to an increase of FOM from 1 to 26, as seen in Fig. 12(c). This value is so far the largest reported FOM achieved in any NIM in the optical region.

Chapter IV. Sub-wavelength Patterning in a Hyperbolic Metamaterials by Volume Plasmon Polaritons (based on papers A7-A10, A14, A22.)

Fourth chapter incudes experiments on optical metamaterials with hyperbolic dispersion. *Hyperbolic* materials enable numerous surprising applications that include far-field subwavelength imaging, nanolithography, and emission life-time engineering. The wavevector of a plane wave in these media follows the surface of a hyperboloid in contrast to an ellipsoid for conventional anisotropic dielectric. The consequences of *hyperbolic dispersion* were first studied in the 50's pertaining to the problems of electromagnetic wave propagation in the Earth's ionosphere and in the stratified artificial materials of transmission lines. Recent years have brought explosive growth in optics and photonics of hyperbolic media based on metamaterials across the optical spectrum.

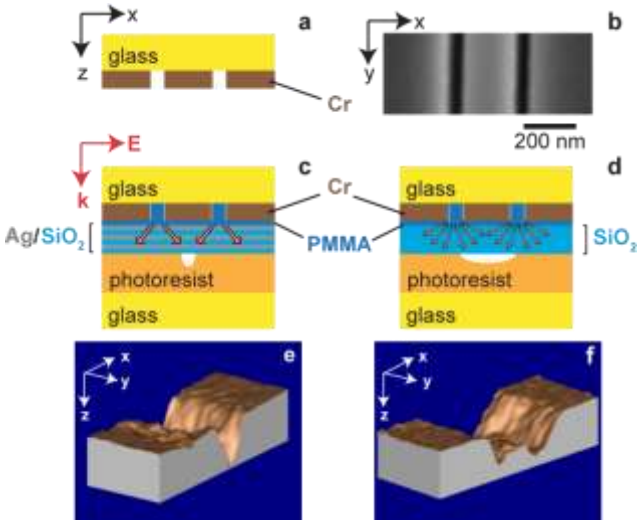

Figure 13. Schematic diagram (a) and a SEM image (b) of the double slit milled in a chromium film. (c**)** Schematic diagram of the double slit with a silver-silica lamellar HMM slab in contact with a photoresist layer. **(**d**)** Schematic diagram of double slit with a reference silica slab in contact with a photoresist layer. Incident and diffracted fields are shown in red. AFM images after develop for the silver-silica lamellar HMM sample (e) and the silica layer sample (f). The dimensions of the images in x axis are 600 nm and 1000 nm for (e) and (f), respectively. The dimensions of the images for (e) and (f) in x and y directions are 1500 nm and 600 nm, respectively.

Inside of a hyperbolic medium, the principal components of the permittivity tensor have opposite signs causing the medium to exhibit a 'metallic' type of response to light waves in one direction, and a 'dielectric' response in the other. Our study shows that inside hyperbolic media, *volume plasmon-polaritons* (VPPs) propagate along the characteristic interfaces of the constitutive materials, forming distinct, directionally dependent optical responses. This is very similar to the propagation of conventional *surface plasmon-polaritons* (SPPs) along the planar interfaces separating the isotropic dielectrics and metallic slabs. E.g., transverse-magnetic (TM) VPPs in a uniaxial medium, $\varepsilon = \mathrm{diag}\ \varepsilon_o, \varepsilon_o, \varepsilon_e$, propagate along the resonance cone between the directions with $\mathrm{Re}\,\varepsilon(\varphi_c) > 0$ and $\mathrm{Re}\,\varepsilon(\varphi_c) < 0$. The Young's double-slit scheme is used to study the spatially-confined diffraction in a hyperbolic slab, made of many thin planar layers of a metal and dielectric, to obtain the sub-wavelength interference pattern of VPPs at the output interface. Proof-of-concept systems for producing such patterns applicable to nanolithography and subwavelength probes are demonstrated in this chapter.

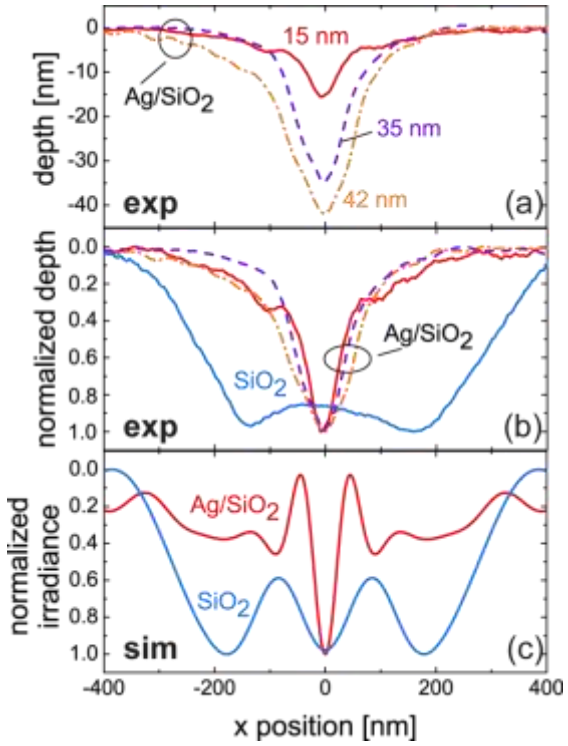

Figure 14. (a) Depth profiles from the AFM scans for the silver-silica lamellar HMM sample having three different depths depending on exposure conditions. (b) Normalized depth profiles of the HMM sample shown in (a) and the silica layer sample. The actual depth for the silica layer sample is 112 nm. (c) Simulated irradiances at the slab-substrate interface for the lamellar HMM slab and the uniform slab of silica.

Fig. 14(a) shows the AFM scans averaged along the slits for the silver-silica lamellar HMM sample deposed for 8 to 10 minutes. When the pattern depth in photoresist is 15 nm, the full-width-at-half-maximum (FWHM) is 83 nm. Longer exposure time resulted in a deeper profile and wider FWHM.

Thus, for the writing depths of 35 nm and 42 nm the FWHMs are 105 nm and 135 nm, respectively. Our results clearly indicate that planar metal-dielectric lamellar structures have the capability to form the diffracted light from the slits into a subwavelength interference spot. In Fig. 14(b), we show the normalized AFM scans presented in Fig. 14(a) as well as the silica layer sample. As the penetration depth (exposure time) increases, the contrast becomes better while the FWHM becomes larger. If the experimental profile was extrapolated to an even smaller depth, the side peaks would grow and the central peak would become narrower, approaching the simulated irradiance just near the resist's surface. Fig.14(c) depicts the irradiances at the interfaces and the substrate obtained from the simulations. The FWHM of the central peaks of the HMM structure and the single layer are 45 nm and 514 nm, respectively. Thus, the numerical simulation results agree with our experimental results.

Chapter V. Scattering Suppression by Epsilon-Near-Zero Plasmonic Fractal Shells

(based on papers A5, A6, A21)

Final, fifth chapter covers experimental demonstration of scattering suppression for the core-shell nanoparticles of about micron size, see Fig.15. Significant extinction from the visible to mid-infrared makes fractal shells very attractive as aerosolized obscurants. In contrast to the planar fractal films, where the absorption and reflection equally contribute to the extinction, the shells' extinction is caused mainly by the absorption. The Mie scattering resonance at 560 nm (Fig,16 left) of a silica core with 780 nm diameter is suppressed by 75% and only partially substituted by the absorption in the shell so that the total transmission is noticeably increased. The silica vibrational stretching band at 9 μm in absorption also disappears. Effective medium theory supports our experiments and indicates that light goes mostly through the epsilon-near-zero shell with approximately wavelength independent absorption rate.

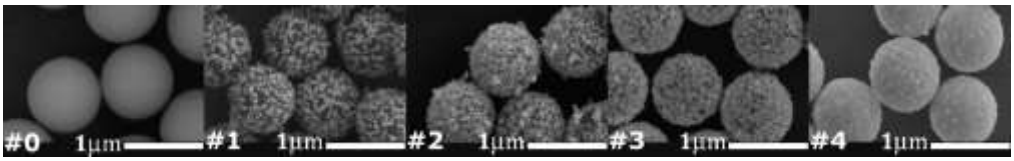

Figure 15: FESEM images of the core-shell particles with different gold shell coverage and morphologies.

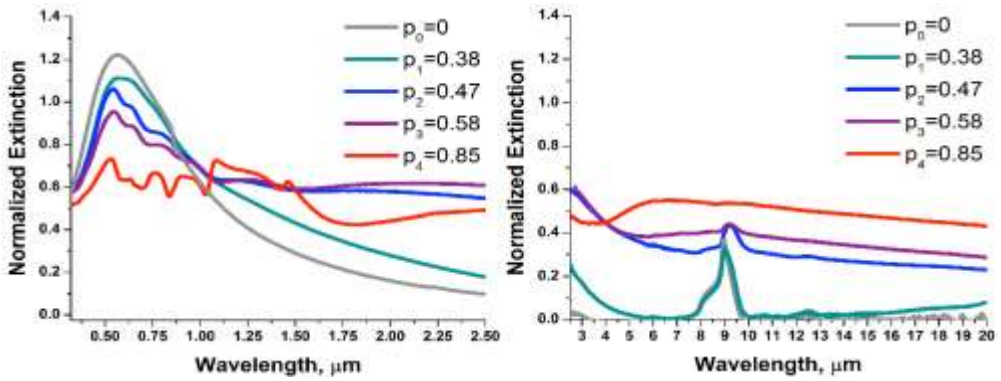

Figure 16: Normalized extinction spectra of the core-shell particles with different gold shell coverage and morphologies shown in Figure 15.

In the experiments, silica microspheres with a diameter of about 780 nm were coated with gold nanostructures using a modified method of the reduction of gold salt, chloroauric acid ($HAuCl_4$) with formaldehyde (CH_2O) in the presence of surfactants and stabilizers. The recipe was modified in order to fabricate fractal semicontinuous shells. Specifically, the gold reduction with formaldehyde was directly performed on the amino functionalized silica microspheres without preliminary seeding. The surface coverage of the gold on the microsphere surface was varied for different samples by varying the reduction time. The solution was stabilized with polyvinylpyrrolidone (PVP) to prevent aggregation of the microspheres. The dissertaion provides more details. The synthesized gold-coated microspheres were then deposited on zinc selenide (ZnSe) substrates for the infrared spectroscopy and on fused silica substrates for spectroscopy in the visible range.

Several different samples have been synthesized to study the effect of the shell structures with gradually increasing gold coverage (p), Fig15. The spectra for normalized extinction (NE) are presented in Figure 16. The normalized transmittance (NT) spectra were first normalized by the transmittance of the bare substrate. Since the density of microspheres on substrate was slightly different for different samples the extinction was normalized per the density. The normalized extinction spectra were calculated as $NE=(-\log NT)/N_S$, where N_S is the core-shell microsphere surface density calculated from the field emission scanning electron microscopy (FESEM) images and taken in μm^{-2}. FESEM images of different shell structures corresponding to the normalized extinction spectra are presented in Figure 15. The samples are labeled from 0 to 4, where 0 corresponds to the sample of bare silica microspheres ($p_0=0$) and 1-4 correspond to the samples with gradually increasing gold coverage in the shells, namely $p_1=0.38\pm0.03$, $p_2=0.47\pm0.01$, $p_3=0.58\pm0.03$, and $p_4=0.85\pm0.02$. Note that the FESEM images allow to measure only 2D projection of the structure and the gold coverage is calculated for such a plane view. That is a good approximation of the resulting filling fraction of metal (f) which we use in the simulations for less dense shells. The samples 3 and 4 can be clearly seen as having 3D structure, and thus the filling fraction can be less than estimated from the plane coverage. The shells have the fractal structure with fractal dimension D=1.75-1.82. It was calculated as the power dependence of the number of gold nanoparticles N_p inside the circle of radius R, $N_p/N_0=(R/R_0)^D$. For the bare silica microspheres there is the absorption peak due to the O-Si-O vibrational stretching band at 9 μm and there is an extinction peak in the visible spectral range due to the Mie scattering resonance at 560 nm (Figure 16 for p=0).

CONCLUSIONS

In the thesis we present experimental feasibility study on optical NIMs, metamagnetics across the visible spectral range, subwavelength photolithography using hyperbolic metamaterials, scattering

suppression with epsilon near-zero fractal shell, and effect of nanostructurering on the metal dielectric function. We have demonstrated, for the first time, feasibility of optical NIMs and losses compensation with gain for NIMs. We should highlight our finding of a new type of plasmonics in magnetic nanoparticles with spin-polarization. The significance of the study can be judged based on the number of citations. It's a one of the parameters to justify the importance of work and impact it has on our research field, and how others may benefit from it. Thus we provide a number of citations according to Scopus for each conclusion below.

1. The Ag dielectric function for moderately sized, about 100 nm, strips differ from that of bulk Ag and is size-dependent for both polarizations of light. Surprisingly, the geometrical effect of roughness is mostly responsible for increased losses at the plasmon resonances of the nanostructure, while the surface roughness does not affect the Ag permittivity. (242 citations for paper A23)

2. Effect of annealing on the nanostructure performance depends on the geometry, and can be positive or negative. In the case of square shape nanoantennas annealing not only increases the grains size but also reduces the reflection coefficient of the potential barriers between grains. Both factors result in substantially improved electron relaxation rate for nanostructures and make it comparable with the large area samples. (146 citations for paper A16; 104 for A19)

3. (a) Our analysis of the $\chi^{(3)}$ values and its size dependence it was concluded that the conduction electron intra-band transitions play a major role, in contrast to the common belief about negligible role of the conduction electrons.

(b) Our results re-affirm the Rautian's model quantum well theory with the Hamiltonian of electron-field interaction taking the form *of* the dipole moment and the electrical field. We found good agreement of the size-dependent $\chi_m^{(3)}$ with the literature experiment. The result that cannot be achieved with a theoretical size dependence derived by Hache, Ricard, and Flytzanis, with the Hamiltonian that uses a description in terms of a vector potential and electron momentum.

(c) We prove the importance of saturation effects for the local field enhancement factor, which strongly affects nonlinear processes and SERS. Therefore, the saturation will be especially important when using high-intensity laser light typical for pulsed fs and ps lasers.

(91 citations for paper A31)

4. Cobalt nanoparticles synthesized by high temperature reduction of cobalt salt show strong plasmon resonance at 280 nm with better quality than that of gold nanoparticles in the visible spectrum. This type of plasmon has unusual properties due to existence of two independent groups of electrons with opposite spins providing weak interaction so that all electron scattering processes occur without spin flip. The scattering with spin flip can be initiated by the domain structure. In fact, our results show an optical analogous of giant magneto-resistance (GMR).

5. For an array of pairs of parallel gold rods, we obtained a negative refractive index of $n' \approx -0.3$ at the optical communication wavelength of 1.5 μm. It was the first experimental demonstration of optical NIMs in this competitive field. (1450 citations for paper A28; 103 for A29)

6. Feasibility of metamagnetics in the visible spectral range was demonstrated for a grating of the

nanostrips pairs. We demonstrate magnetic resonant behavior ranging from 491 nm to 754 nm, covering the visible spectrum. The permeability ranges from -1.6 at 750 nm to 0.5 at 500 nm. (246 citations for paper A24; 180 for A26).

7. Negative refractive index has been demonstrated at the optical wavelengths using paired crossed gratings arrays (fishnets). It has been done to demonstrate a double negative-NIM response at wavelengths as short as 813 nm. The sample showed a maximum FOM (figure of merit) of 1.3 with $n' \approx -1.3$. We have also reported the shortest wavelength at which NIM behavior has been observed. The sample displayed a single negative-NIM response at 710 nm with a maximum FOM of 0.5 with $n' \approx -0.6$. (180 citations for paper A25; 142 for paper A17).

8. (a) We have experimentally demonstrated an active negative-index metamaterial. Our results for the first time solve the inherent problem of loss in negative-index metamaterials made from nanostructured metal-dielectric composites.

(b) The efficiency of the loss compensation in our sample arises from the local-field enhancement of the structure when a gain medium is used as the spacer layer. Measured the effective extinction coefficients at 737 nm are $\alpha \approx 6.75 \times 10^{3} cm^{-1}$ and $\alpha = 1.13 \times 10^{5} cm^{-1}$ for the device with and without gain. Thus the effective amplification is $\alpha = -1.07 \times 10^{5} cm^{-1}$, which is 46 times larger at this wavelength than the "seed" value (without the local-field factor) that was used in simulations. (646 citations for paper A15; 119 for paper A27).

9. We have experimentally shown that diffracted light propagates inside a hyperbolic material made of a planar silver-silica lamellar structure along the resonance cone boundary along the direction, where $\mathrm{Re}\,\varepsilon(\varphi_c) > 0$ switch to $\mathrm{Re}\,\varepsilon(\varphi_c) < 0$. Such propagation across the real metal-dielectric interfaces is a characteristic feature of the volume plasmon-polaritons. The interference of VPPs from a double-slit creates a sub-wavelength interference pattern, which is six times smaller than the free space wavelength at 465 nm. This is in sharp contrast to the double-slit experiment in silica, which results in a diffraction-limited pattern. Such unique subwavelength interference patterns offered by hyperbolic metamaterials allow for applications in nano-photolithography demonstrated in our work. (239 citations for paper A7; 140 for paper A9; 130 for paper A8; 73 for paper A14.)

10. (a) Our experiments show that the optical response of the core-shell microsphere with a gold fractal shell is dominated by the shell absorption. Similar to the planar fractal films, the absorption is enhanced in the broad spectral range up to $20\,\mu\mathrm{m}$. It is interesting though that the specular reflection and back-scattering are relatively small for the fractal shells due to 3D spherical geometry.

(b) What is counterintuitive is that the resulting transmission cross-section for the core with gold shell is higher than the bare silica core at the Mie resonance wavelength. This is due to the forward scattering suppression of silica microspheres by adding the plasmonic gold shells. We prove that

the absorption in the shell contributes the most to the extinction of the whole core-shell microsphere.

(c) Another surprising result is that the Mie scattering resonance at 560 nm of a silica core with 780 nm diameter is suppressed by 75% and partially substituted by the absorption in the shell so that the total transmission is increased by factor of 1.6 due to the gold fractal shell.

(d) The calculated effective permittivity of the gold shell manifests the epsilon-near-zero condition over the whole spectral range under study. The O-Si-O vibrational stretching band of the core in the mid-infrared spectral range, is "invisible" in the spectra of the core-shell extinction. These observations for the visible and mid-IR spectra indicate that the light goes mostly through the epsilon-near-zero shell with approximately wavelength independent absorption rate. Thus the fractal films being synthesized on the microspheres show interesting properties of "guiding" light through the shell. (38 citations for paper A21.)

REFERENCES:

[1]. Veselago, V.G., 1968, The electrodynamics of substances with simultaneously negative values of ε and μ, Soviet Physics Uspekhi 10(4), 509-514.

[2]. A. N. Lagarkov, A. K. Sarychev, and A. P. Vinogradov, Pis'ma Zh. Éksp. Teor. Fiz. 40, 296 (1984) [JETP Lett. 40, 1083 (1984)].

[3]. A. N. Lagarkov, V.N. Semenenko, V.A. Chistyaev, D.E. Ryabov, S.A. Tretyakov, and K.R. Simovski, Electromagnetics 17, 213 (1997).

[4]. J. B. Pendry et al., IEEE Trans. Microwave Theory Tech. 47, 2075 (1999).

[5]. A. P. Vinogradov, A. A. Kalachev, A. N. Lagarkov, V. E. Romanenko, G. V. Kazantseva, Spatial dispersion effects in composite materials in microwave, Dokl. Akad. Nauk, 1996, Volume 349, Number 2, 182–184

[6]. A. P. Vinogradov, On the form of constitutive equations in electrodynamics, Physics Uspekhi 45 (3), 331 – 338, (2002).

[7]. A.N. Lagarkov, V.N. Kisel, Dokl. Ross. Akad. Nauk 377 1 (2001) [Phys. Dokl. 46 163 (2001)].

[8]. Smith, D.R., Padilla, W., Vier, J.D.C., Nemat-Nasser, S.C., Schultz, S., 2000, Composite medium with simultaneously negative permeability and permittivity, Phys. Rev. Lett. 84, 4184--4187.

[9]. Shelby, R.A., Smith, D.R., Schultz, S., 2001, Experimental verification of a negative index of refraction, Science 292, 77-79.

[10]. Pendry, J.B., 2000, Negative refraction makes a perfect lens, Phys. Rev. Lett. 85, 3966-3969.

[11]. Fang, N., Lee, H., Zhang, X., 2005, Sub-diffraction-limited optical imaging with a silver superlens, Science 308, 534-537.

[12]. Melville, 0.0.S., Blaikie, R..J., 2005, Super-resolution imaging through a planar silver layer, Opt. Expr. 13, 2127-2134.

[13]. Linden, S., Enkrich, C., Wegener, M., Zhou, J., Koschny, T., Soukoulis, C.M., 2004, Magnetic response of metamaterials at 100 terahertz, Science 306, 1351-1353.

[14]. Yen, T.J., Padilla, W.J., Fang, N., Vier, D.C., Smith, D.R., Pendry, J.B., Basov, D.N., and Zhang, X . 2004, Terahertz magnetic response from artificial materials, Science 303, 1494-1496.

[15]. Zhang, S., Fan, W., Minhas, B.K., Frauenglass, A., Malloy, K.J., Brueck, S.R.J., 2005, Midinfrared resonant magnetic nanostructures exhibiting a negative permeability. Phys. Rev. Lett. 94(037402), 1-4.

[16]. Podolskiy, V.A., Sarychev, A.K., Shalaev, V.M., 2002, Plasmon modes in metal nanowircs and left-handed materials, J. Nonlinear Opt. Phys. Mat. 11, 65-74.

[17]. Podolskiy, V.A., Sarychev, A.K., Shalaev, V.M., 2003, Plasmon modes and negative refraction in metal nanowire composites, Opt. Expr. 11, 735-745.

[18]. Podolskiy, V.A., Sarychev, A.K., Narimanov, E.E., Shalaev, V.M., 2005, Resonant light interaction with plasmonic nanowire systems, J. Opt. A Pure Appl. Opt. 7, S32-S37.

[19]. Shalaev, V.M., Cai, W., Chettiar, U., Yuan, H.-K., Sarychev, A.K., Drachev. V.P., Kildishev, A.V., 2005, Negative index of refraction in optical metamaterials, Opt. Lett. 30, 3356-3358;

[20]. Drachev, V.P., Cai, W., Chettiar, U., Yuan, H.-K., Sarychev, A.K., Kildishev, A.V., Shalaev, V.M., 2006, Experimental verification of optical negative-index materials, Laser Phys. Lett. 3, 49-55/001 10.1002/lapl.200510062.

[21]. Kildishev, A.V., Cai, W., Chettiar, U., Yuan, H.-K., Sarychev, A.K., Drachev. V.P. Shalaev. V.M., 2006, Negative refractive index in optics of metal-dielectric composites, J. Opt. Soc. Am. B 23, 423-433 (2006).

[22]. P. B. Johnson and R. W. Christy, "Optical constants of the noble metals," Phys. Rev. B **6**, 4370 (1972).

[23]. D. W. Lynch and W. R. Hunter, in *Handbook of Optical Constants of Solids*, E. D. Palik, ed. (Academic Press: New York, 1985).

[24]. Mayadas, A. F.; Shatzkes, M.; Janak, J. F., Electrical Resistivity Model for Polycrystalline Films - Case of Specular Reflection at External Surfaces. *Applied Physics Letters* **1969,** 14, (11), 345-&.

[25]. Motulevich, G. P.; Malyshev, V. I.; Skobeltìsyn, D. V., *Optical properties of metals*. Consultants Bureau: New York,, 1973; p ix, 228 p.

[26]. S. G. Rautian, Sov. Phys. JETP, **85**, 451-461 (1997).

[27]. K. Uchida, S. Kaneko, S. Omi, C. Hata, H. Tanji, Y. Asahara, and A. J. Ikushima, J. Opt. Soc. Am. B **11**, 1236 (1994).

[28]. F. Hache, D. Ricard, and Flytzanis, J. Opt. Soc. Am. B **3**, 1647 (1986).

[29]. Tsymbal, E.Y.; Pettifor, D.G. *Perspectives of Giant Magnetoresistance*. in Ehrenreich, H. & Spaepen, F. (Eds): Solid state physics **,** (Academic Press, Boston), 56, pp. 113-237 (2001). http://digitalcommons.unl.edu/physicstsymbal/50

[30]. Gall, D. *J. App. Phys.* **2016**, 119, 085101-085101-5 .

[31]. Bergman, D. J.; Stroud, D. *Properties of macroscopically ingomogeneous media*, in Ehrenreich, H. &Turnbull, D. (Eds): Solid state physics **,** (Academic, Boston), 46, pp. 149-270 (1992).

[32]. Markel, V. A.; Muratov, L. S.; Stokman, M. I. Optical properties of fractals: theory and numerical simulation. *Sov. Phys. JETP* **71**(3), 455-464 (1990).

[33]. D. R. Smith, S. Schultz, P. Markoŝ, and C. M. Soukoulis, "Determination of effective permittivity and permeability of metamaterials from reflection and transmission coefficients," Phys. Rev. B **65**, 195104 (2002).